Geoscience Frontiers xxx (2017) 1–20

HOSTED BY

Contents lists available at ScienceDirect

China University of Geosciences (Beijing)

Geoscience Frontiers

journal homepage: www.elsevier.com/locate/gsf

Research Paper

Meso-Cenozoic tectonic evolution of the Talas-Fergana region of the Kyrgyz Tien Shan revealed by low-temperature basement and detrital thermochronology

Simon Nachtergaele [a,*], Elien De Pelsmaeker [a], Stijn Glorie [b], Fedor Zhimulev [c], Marc Jolivet [d], Martin Danišík [e], Mikhail M. Buslov [c], Johan De Grave [a]

[a] Laboratory for Mineralogy and Petrology, Department of Geology, Ghent University, Ghent, Belgium
[b] Tectonics, Resources and Exploration (TraX), Department of Earth Sciences, University of Adelaide, Adelaide, Australia
[c] Institute of Geology & Mineralogy, Siberian Branch, Russian Academy of Sciences, Novosibirsk, Russia
[d] Université de Rennes 1, Laboratoire Géosciences Rennes, UMR 6118 CNRS, Rennes, France
[e] John de Laeter Centre, Applied Geology, TIGeR, Curtin University, Perth, 6846, Australia

ARTICLE INFO

Article history:
Received 4 July 2017
Received in revised form
13 October 2017
Accepted 15 November 2017
Available online xxx
Handling Editor: C.J. Spencer

Keywords:
Tian Shan
Central Asian Orogenic Belt
Thermal history modelling
Apatite fission track dating
Zircon (U–Th)/He dating

ABSTRACT

This study provides new low-temperature thermochronometric data, mainly apatite fission track data on the basement rocks in and adjacent to the Talas-Fergana Fault, in the Kyrgyz Tien Shan in the first place. In the second place, we also present new detrital apatite fission track data on the Meso-Cenozoic sediments from fault related basins and surrounding intramontane basins. Our results confirm multi-staged Meso-Cenozoic tectonic activity, possibly induced by the accretion of the so-called Cimmerian blocks to the Eurasian margin. New evidence for this multi-staged thermo-tectonic activity is found in the data of both basement and Meso–Cenozoic sediment samples in or close to the Talas-Fergana Fault. Zircon (U–Th)/He and apatite fission track data constrain rapid Late Triassic–Early Jurassic and Late Jurassic–Early Cretaceous basement cooling in the Kyrgyz Tien Shan around 200 Ma and 130–100 Ma respectively. Detrital apatite fission track results indicate a different burial history on both sides of the Talas-Fergana Fault. The apatite fission track system of the Jurassic sediments in the Middle Tien Shan unit east of the Talas-Fergana Fault is not reset, while the Jurassic sediments in the Fergana Basin and Yarkand-Fergana Basin, west of the fault zone, are partially and in some cases even totally reset. The totally reset samples exhibit Oligocene and Miocene ages and evidence the Cenozoic reactivation of the western Kyrgyz Tien Shan as a consequence of the India-Eurasia convergence.

1. Introduction

The Tien Shan (or Tian Shan) is a 2500 km long intracontinental mountain belt located in northwest China, Kyrgyzstan, Kazakhstan, Tajikistan and Uzbekistan and forms the southwest part of the Central Asian Orogenic Belt (CAOB) (Fig. 1). The CAOB represents a mosaic of Precambrian and Palaeozoic blocks, accreted during the closure of the Paleo-Asian ocean (Sengör et al., 1993; Filippova et al., 2002; Khain et al., 2003; Konopelko et al., 2007; Windley et al., 2007; Xiao et al., 2008; Glorie et al., 2011; De Grave et al., 2012; Wilhem et al., 2012). During the Mesozoic and Cenozoic, parts of the CAOB were reactivated in response to far-field accretion-collision events along the (Eur)Asian margin, with a final and still active late Cenozoic phase related to the India-Eurasia collision (Molnar and Tapponier, 1975; Watson et al., 1987; Dumitru et al., 2001; De Grave et al., 2007; Jolivet et al., 2010; De Pelsmaeker et al., 2015; Glorie and De Grave, 2016; Käßner et al., 2016, 2017). During these reactivation phases, deformation is often partitioned along inherited, weak crustal structures (Yin and Harrison, 2000; Dumitru et al., 2001; Aitchison et al., 2007; Kapp et al., 2007; Glorie et al., 2010; Wack et al., 2014; Jolivet, 2015). In this context, the currently active 500 km long NW–SE oriented intracontinental dextral strike-slip Talas-Fergana Fault (TFF) is an important inherited Palaeozoic structure and has generated an

* Corresponding author. Department of Geology, Ghent University, Krijgslaan 281.S8, WE13, B-9000 Ghent, Belgium.
E-mail address: Simon.Nachtergaele@UGent.be (S. Nachtergaele).
Peer-review under responsibility of China University of Geosciences (Beijing).

https://doi.org/10.1016/j.gsf.2017.11.007

estimated accumulated offset of more than 100 km since the end of the Palaeozoic (Burtman et al., 1996; Konopelko et al., 2013; Rolland et al., 2013; Bande et al., 2015b; Burtman, 2015; Alexeiev et al., 2017) (Figs. 1 and 2). The fault represents the southern part of the larger Karatau– Talas–Fergana Fault that extends from southern Turgay in Kazakhstan to western Tarim in China. The TFF has evolved in three discrete phases of deformation, during three stages: (1) in the late Permian and Early Triassic; (2) in the Early and Middle Jurassic; and (3) in the late Cenozoic (Thomas et al., 1993; Burtman et al., 1996; Sobel, 1999; Allen et al., 2001; Konopelko et al., 2013; Rolland et al., 2013; Bande et al., 2015b; Alexeiev et al., 2017), but the timing of the associated crustal exhumation is still poorly understood. This study aims to better constrain the Meso-Cenozoic tectonic evolution of the TFF and the tectonic response of the adjacent basement blocks in terms of exhumation and associated mountain building, erosion and sediment accumulation in the nearby intramontane basins.

The first part of this study presents new low-temperature thermochronological data from basement blocks along and near the TFF, i.e. 20 apatite fission track (AFT) ages, 2 zircon (U–Th)/He ages, 1 apatite U–Pb age and the associated thermal history models. The second part of this study presents 17 new detrital AFT ages and confined track length data of 5 samples from Mesozoic and early Cenozoic sediments, obtained from the surrounding intramontane Tien Shan basins: Fergana, Yarkand-Fergana and Ming-Kush-Kökömeren basins (Figs. 1 and 2). The analysed sediment samples fit in detailed sedimentary logs of De Pelsmaeker et al. (2018) and for 11 of the 17 analysed samples it was possible to compare the obtained AFT results with the zircon U–Pb results from the same detrital sample. Hence, we present this new multi-method chronological data and integrate them with existing results for the Tien Shan (Dumitru et al., 2001; Sobel et al., 2006a,b; De Grave et al., 2007, 2011a, 2012, 2013; Glorie et al., 2010, 2011; Jolivet et al., 2010; Macaulay et al., 2014; Bande et al., 2015b, 2017; Glorie and De Grave, 2016) to gain more insights in the Meso-Cenozoic reactivation and burial history of the region.

2. Geological setting

2.1. Pre-Mesozoic evolution

Paleozoic complexes in the Kyrgyz Tien Shan are traditionally divided into three major tectonic units: Northern Tien Shan (NTS), Middle Tien Shan (MTS) and Southern Tien Shan (STS) (e.g. Windley et al., 2007; Konopelko et al., 2008; Seltmann et al., 2011; Alexeiev et al., 2016) (Fig. 2). The NTS mainly consists of Precambrian continental fragments related to the Kazakhstan paleocontinent (e.g. Kröner et al., 2013). The basement is extensively intruded by Cambrian to Silurian granitoids related to major collisions

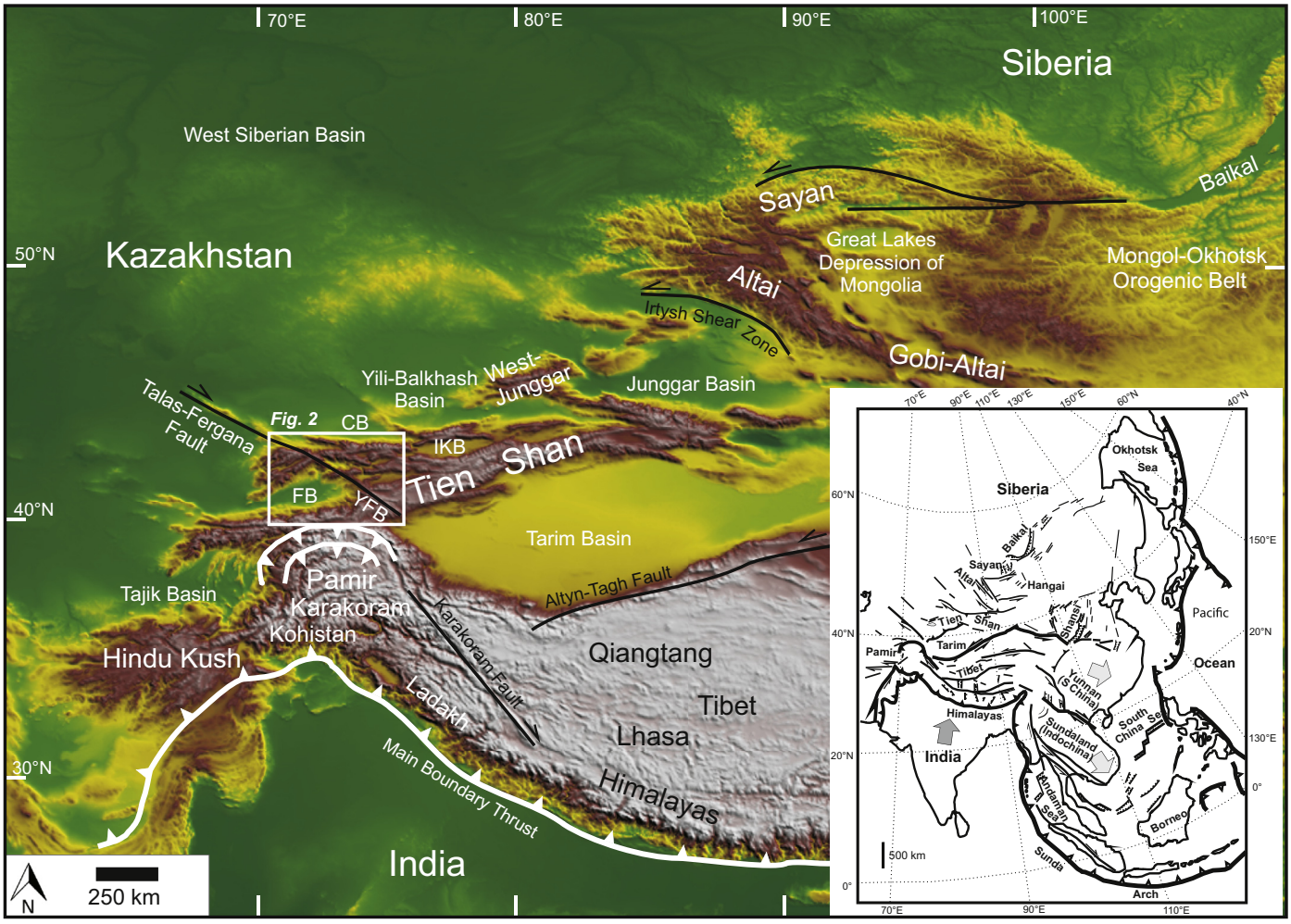

Figure 1. General topographic and tectonic map of Central Asia with indication of the study area (white box detailed in Fig. 2). CB = Chu Basin, FB = Fergana Basin, IKB = Issyk-Kul Basin, YFB = Yarkand-Fergana Basin (adapted from De Grave et al., 2007; De Pelsmaeker et al., 2015).

Please cite this article in press as: Nachtergaele, S., et al., Meso-Cenozoic tectonic evolution of the Talas-Fergana region of the Kyrgyz Tien Shan revealed by low-temperature basement and detrital thermochronology, Geoscience Frontiers (2017), https://doi.org/10.1016/j.gsf.2017.11.007

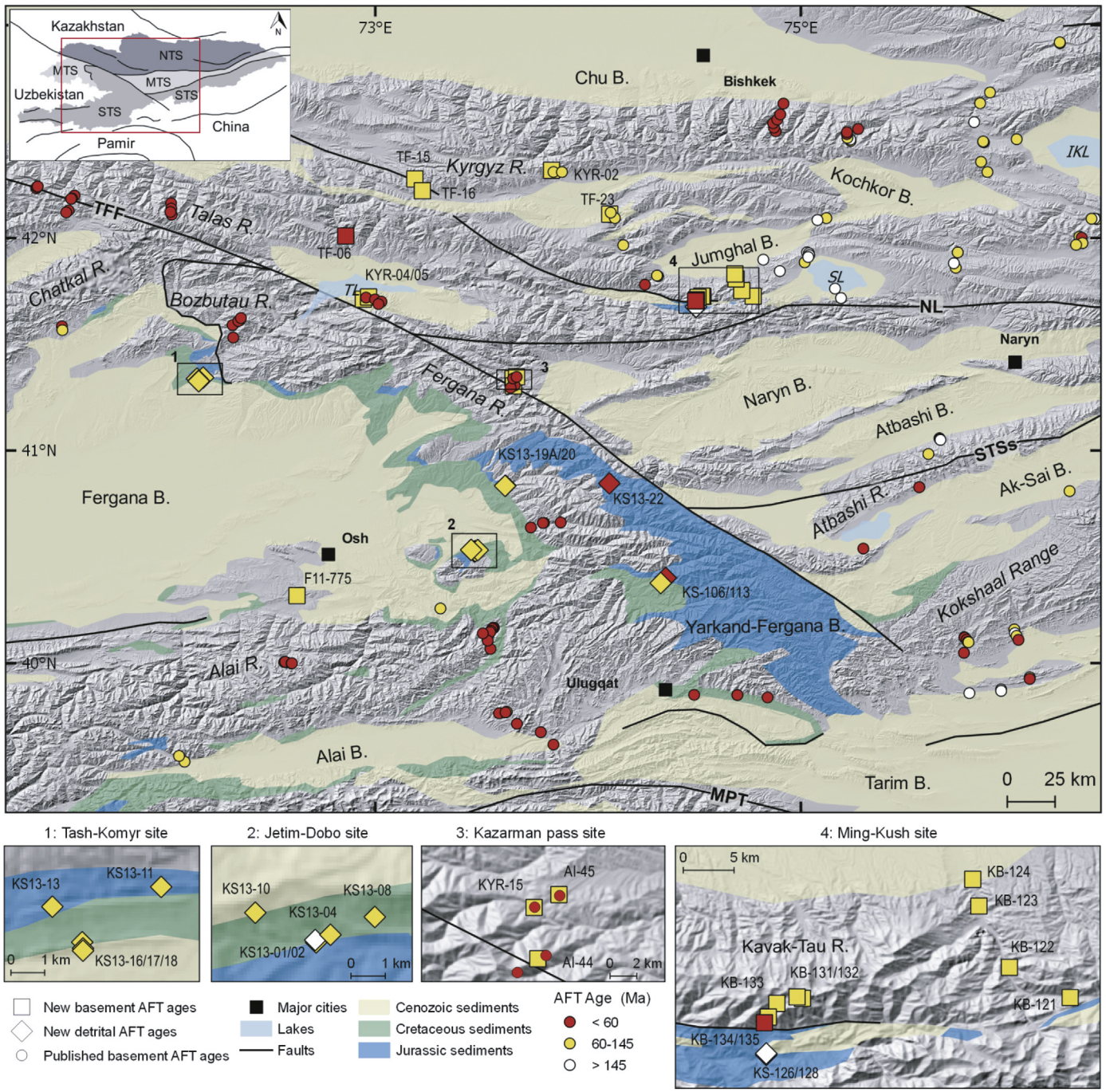

Figure 2. Shaded relief map of the study area with indication of the sample locations and Jurassic, Cretaceous and Cenozoic sediments. Non-coloured areas represent the crystalline and pre-Mesozoic basement. Detail maps: (1) Tash-Komyr site (Fergana Basin); (2) Jetim-Dobo site (Fergana Basin); (3) Kazarman pass site; (4) Ming-Kush site. Compilation of available published apatite fission-track (AFT) ages from crystalline and pre-Mesozoic basement rocks is based on data from Sobel et al. (2006a, b), Glorie et al. (2010, 2011), De Grave et al. (2011a, 2012, 2013), Macaulay et al. (2013, 2014), Bande et al. (2015a, 2017), Käßner et al. (2016) and are indicated as circles. Squares reflect new crystalline and pre-Mesozoic AFT ages and diamonds reflect new detrital AFT ages from this study. Colours of the symbols indicate the age range as shown on the map. NL = Nikolaev Line, TFF = Talas-Fergana Fault, STSs = South Tien Shan suture, MPT = Main Pamir Thrust, NTS = North Tien Shan, MTS = Middle Tien Shan, STS = South Tien Shan, SL = Song-Kul lake, IKL = Issyk-Kul lake, TL = Toktogul lake.

associated with the formation of the Kazakhstan paleocontinent (Glorie et al., 2010; Kröner et al., 2013; Alexeiev et al., 2016). The NTS is additionally affected by Late Devonian–Carboniferous magmatism associated with the evolution of a continental magmatic arc, and by Early Permian post-collisional granitoids (Konopelko et al., 2008; Biske and Seltmann, 2010; Kröner et al., 2013). The NTS is now separated from the MTS by the E–W oriented Nikolaev Line, which represents a combination of late Paleozoic thrusts and strike-slip faults (Fig. 2). To some extent it runs sub-parallel to the Ordovician Terskey suture (e.g. Burtman, 2010). The NTS and MTS units were welded together during the Middle Ordovician and subsequently evolved as the southern margin of the Kazakhstan paleocontinent. The MTS represents a collage of Precambrian microcontinental fragments in the north

Please cite this article in press as: Nachtergaele, S., et al., Meso-Cenozoic tectonic evolution of the Talas-Fergana region of the Kyrgyz Tien Shan revealed by low-temperature basement and detrital thermochronology, Geoscience Frontiers (2017), https://doi.org/10.1016/j.gsf.2017.11.007

and an Ordovician arc in the south (e.g. Alexeiev et al., 2016; Kröner et al., 2017). The microcontinental fragments consist of Paleoproterozoic gneisses, Neoproterozoic granitoids and felsic volcanic rocks, overlain by Neoproterozoic to Ordovician passive margin sediments. In addition, Permian (post-)collisional igneous rocks, related to the closure of the late Paleozoic Turkestan Ocean, were emplaced in the MTS (Konopelko et al., 2007; Biske and Seltmann, 2010; Jolivet et al., 2010; Seltmann et al., 2011; De Grave et al., 2013; Liu et al., 2014) (Fig. 2). The Turkestan Ocean was an oceanic branch that still separated Paleo-Kazakhstan from Tarim at that time (e.g. Windley et al., 2007). In central Kyrgyzstan, the MTS and STS are separated by the ophiolite-bearing Atbashi-Inylchek or South Tien Shan suture which formed around 310–280 Ma (e.g. Konopelko et al., 2007; Loury et al., 2016).

The STS represents a late Paleozoic accretionary complex and collisional belt (with Silurian to Lower Permian sediments and igneous rocks) related to the Pennsylvanian closure of the Turkestan Ocean (320–300 Ma) and collision of Kazakhstan (including the NTS and MTS) with the Tarim microcontinent (Windley et al., 2007; Alekseev et al., 2009; Biske and Seltmann, 2010; Biske et al., 2013; Liu et al., 2014; Burtman, 2015; Alexeiev et al., 2016; Käßner et al., 2016; Loury et al., 2016). This Turkestan closure led to the final assembly of the ancestral Tien Shan and was accompanied by significant collisional and post-collisional magmatism. Subsequently, the entire Tien Shan experienced transpressive deformation during the Permian–Early Triassic, which was responsible for dispersed rotations and shear movements along strike-slip faults (e.g. Bazhenov et al., 1999; Van der Voo et al., 2006; Rolland et al., 2013; Burtman, 2015). One of the most prominent faults is the NW–SE oriented Talas-Fergana Fault (TFF), that intersects the NTS, MTS and STS (Fig. 2). The TFF played an important role in the post-Paleozoic evolution of the Tien Shan.

2.2. Mesozoic and Cenozoic intracontinental evolution

During the Mesozoic and Cenozoic the region was repeatedly reactivated as a result of collision-accretion events at the (Eur)Asian margins (Sengör, 1984; Watson et al., 1987; Hendrix et al., 1992; De Grave et al., 2007, 2011a, 2013; Jolivet et al., 2010, 2013; Jolivet, 2015). The extent and context of these reactivation events can be traced by studying basement exhumation, associated erosion and sediment accumulation in the nearby basins using multi-chronometric methods (Dumitru et al., 2001; Sobel et al., 2006b; De Grave et al., 2007, 2013; Jolivet et al., 2013; Macaulay et al., 2014; Yang et al., 2014; Tang et al., 2015; Käßner et al., 2016; Zhang et al., 2016; Wang et al., 2017). Previous and ongoing research link distinct Mesozoic basement exhumation phases to the protracted accretion of peri-Gondwanan 'Cimmerian' blocks to the southern Eurasian margin (e.g. Hendrix et al., 1992; De Grave et al., 2007; Angiolini et al., 2013; Glorie and De Grave, 2016). It includes the collision of the Qiangtang block during the Late Triassic–Early Jurassic, the Lhasa block during the Late Jurassic–Early Cretaceous and the less well-understood Karakoram and Kohistan-Ladakh arc during the Late Cretaceous (e.g. Sengör, 1984; Watson et al., 1987; Kapp et al., 2007; Roger et al., 2010; Jolivet, 2015; Gillespie et al., 2017).

In the Early Mesozoic, the Tien Shan acted as an uplifted, physiographic barrier between the Junggar and Kazakh basins to the north, and the Tarim Basin to the south (Carroll et al., 1995; Hendrix, 2000; Jolivet, 2015). The Tarim and Junggar basins (Fig. 1) accumulated a significant amount (~5 km) of Mesozoic sediments (Hendrix, 2000), while in the Kyrgyz Tien Shan sedimentation was limited to smaller, isolated basins. In the Kyrgyz Tien Shan, the Mesozoic sedimentary record starts in the Early–Middle Jurassic. The Yarkand-Fergana Basin (Fig. 2) accumulated the most Jurassic sediments (locally >3 km), related to contemporaneous tectonic activity along the TFF (Belgovskiy et al., 1958; Hendrix et al., 1992; Allen et al., 2001; De Pelsmaeker et al., 2018). During the Early and Middle Jurassic, strike-slip deformation occurred along the TFF, which is related to the formation of the NW–SE striking South Turgay, Leontiev Graben and Yarkand-Fergana releasing bend and pull-apart basins (Burtman et al., 1996; Sobel, 1999; Allen et al., 2001; Yin et al., 2012; Alexeiev et al., 2017). Elsewhere in the Kyrgyz Tien Shan, the Early to Middle Jurassic sedimentary deposits are thinner, more condensed, and comprises organic-rich fluvial and lacustrine strata with a maximum thickness of a few hundred meters (Hendrix et al., 1992; Bachmanov et al., 2008; De Pelsmaeker et al., 2018). Studies indicate that after a rapid basement exhumation phase during the Late Triassic–Early Jurassic, the Tien Shan underwent significant peneplanation. Low-temperature thermochronological research on the Song Kul plateau yielded AFT ages ranging between 206 and 183 Ma and titanite FT ages between 231 and 193 Ma (De Grave et al., 2011a) (Fig. 2). This rapid Late Triassic–Early Jurassic cooling phase is only locally preserved in the basement rocks, and is likely related to the accretion of the Qiangtang–Kunlun terranes to the Eurasian margin in the Late Triassic (Sengör, 1984; Yin and Harrison, 2000; Schwab et al., 2004; De Grave et al., 2011a; Jolivet, 2015; Glorie and De Grave, 2016).

During the Late Jurassic–Early Cretaceous, almost no sediments were deposited or preserved in the Kyrgyz Tien Shan east of the TFF; while to the west, in the Fergana and Yarkand-Fergana basins, sedimentation still continued but the sediments are deposited in a shallower depositional environment compared to the Early–Middle Jurassic setting (e.g. De Pelsmaeker et al., 2018). In the Fergana Basin, thick alluvial fan conglomerates are deposited during the Jurassic–Cretaceous transition. Similar conglomerates also occur in the Junggar and Tarim basins and can be explained by the combined effects of a renewed compressive phase and a regional aridification event (Hendrix et al., 1992; Hendrix, 2000; Jolivet et al., 2013, 2015; Jolivet, 2015; De Pelsmaeker et al., 2018). A renewed compressional phase is also documented by a (locally preserved) Late Jurassic–Early Cretaceous basement cooling episode, with few AFT and ZHe ages of ~160–130 Ma and a more abundant population around ~130–100 Ma (Fig. 2; Glorie and De Grave, 2016, and references therein). Basement cooling in the Kyrgyz Tien Shan in the Early Cretaceous (e.g. De Grave et al., 2012) might be linked to the closure of the Bangong Ocean between Lhasa and the Qiangtang blocks around 130 Ma (Zhu et al., 2016) and subsequent slab break off around ~110 Ma (Kapp et al., 2007; Zhu et al., 2011, 2016; Chen et al., 2014). Furthermore, influence of the diachronous closure of the Mongol-Okhotsk during the Jurassic–Cretaceous, connecting Mongolia and North China to Siberia might have had an influence (Zorin, 1999; Metelkin et al., 2010, 2012; Wilhem et al., 2012), although it is thought that this event mainly affected the areas to the northeast of the Tien Shan, such as the Altai-Sayan region (De Grave et al., 2007, 2009; Glorie et al., 2012a; Jolivet et al., 2013; Glorie and De Grave, 2016).

During the Late Cretaceous–Early Paleogene, the sedimentary record in the Fergana and Yarkand–Fergana basins is characterized by alluvial plain and shallow lake deposits with some marine incursions; while the Tien Shan east of the TFF was likely characterized by a slowly eroding, relatively flat topography where continental sedimentation resumed during the early Paleogene (Burtman et al., 1996; Sobel, 1999; Bosboom et al., 2015).

The most recent reactivation of the Kyrgyz Tien Shan initiated in the late Oligocene–Miocene and is a far-field effect of the ongoing India–Eurasia convergence and subsequent collision (Molnar and Tapponier, 1975). This event affected major fault zones in the Tien Shan, including the TFF (Burtman et al., 1996; Bande et al., 2015b,

Please cite this article in press as: Nachtergaele, S., et al., Meso-Cenozoic tectonic evolution of the Talas-Fergana region of the Kyrgyz Tien Shan revealed by low-temperature basement and detrital thermochronology, Geoscience Frontiers (2017), https://doi.org/10.1016/j.gsf.2017.11.007

2017; Jia et al., 2015; Alexeiev et al., 2017), and is recorded in low-temperature thermochronological data as well (Yin and Harrison, 2000; Sobel et al., 2006a,b; De Grave et al., 2007; Glorie et al., 2010, 2011; Macaulay et al., 2014; Bande et al., 2015b, 2017; De Pelsmaeker et al., 2015; Wang et al., 2017). It is equally well documented in the sedimentary record by the accumulation of thick continental deposits from high-energetic sedimentary settings since the Late Oligocene (Burtman et al., 1996; Bande et al., 2015a,b; W. Yang et al., 2015). Studies of Burtman et al. (1996), Korzhenkov et al. (2014) and Trifonov et al. (2015) indicate that the TFF is still active with an average slip rate estimated at ~9–14 mm/a based on radiocarbon dating of terraces displaced by the fault.

3. Methods

3.1. Apatite fission track dating

3.1.1. General principles

Apatite fission track (AFT) dating is a low-temperature thermochronological method based on the spontaneous nuclear fission of ^{238}U, which is present as trace element in the crystal lattice of apatite. This process produces sub-microscopic linear radiation damage tracks (or fission tracks) in the crystal lattice. These are then chemically etched in order to reveal the tracks for optical microscopic analysis. At temperatures (T) lower than ca. 60 °C, fission tracks in apatite are considered stable on geological time scales, whereas at $T >$ ~120 °C the crystal lattice regenerates and the fission tracks anneal rapidly (e.g. Wagner and Van den haute, 1992; Ketcham et al., 1999). The 60–120 °C temperature window (±2–4 km crustal depth) is referred to as the Apatite Partial Annealing Zone (APAZ). In the 60–120 °C window, tracks can accumulate but are progressively shortened (i.e. partial annealing). The rate of this process depends partly on the chemical composition of the apatite crystal (Green et al., 1989; Wagner and Van den haute, 1992; Carlson et al., 1999; Barbarand et al., 2003). The AFT age, based on the measurement of the spontaneous fission track density, hence dates the time since fission tracks became thermally stable by cooling of the apatite-bearing rock through the APAZ. All samples were analysed with the external detector (ED) method using thermal neutron irradiation, following the standard procedure from the AFT laboratory at Ghent University (e.g. described by De Grave and Van den haute, 2002; De Grave et al., 2009, 2011a; Glorie et al., 2010). Spontaneous fission tracks in apatite were etched in a 2.5% HNO_3 solution for 70 s at 22 °C (analysts J. De Grave and S. Glorie) or in a 5.5 M HNO_3 solution for 20 s at 21 °C (analysts E. De Pelsmaeker and S. Nachtergaele). Induced tracks were revealed in the muscovite ED with 40% HF for 40 min at 20 °C. Irradiation was carried out in the Belgian Reactor 1 (BR1) facility of the Belgian Nuclear Research Centre in Mol. Obtained AFT ages are calculated using the Overall Mean Weighted Zeta using Durango (McDowell et al., 2005) and Fish Canyon Tuff (Hurford and Hammerschmidt, 1985) apatite age standards and IRMM 540 glass dosimeters (De Corte et al., 1998), and are reported as conventional mean zeta-ages (Hurford and Green, 1983; Hurford, 1990) for the basement samples and as central ages (Vermeesch, 2009) for the detrital samples (Section 3.1.2).

In addition to the AFT age, the track length distribution is often used to determine the nature of the cooling paths and allows the reconstruction of the time–temperature history of the basement rocks by thermal history modelling (Ketcham et al., 1999, 2007; Gallagher, 2012). Where possible, a minimum of 100 horizontal confined tracks for each basement sample were measured on 1250× magnification with a KONTRON-MOP-AMO3 digitizing tablet to construct length-frequency distributions. For some samples, no length data was available due to low spontaneous track densities and/or a low number of suitable grains.

Thermal history modelling was performed on basement samples with a sufficient number (~50 or ideally 100) of lengths using the QTQt software from Gallagher (2012), the Ketcham et al. (2007) annealing equations and the Monte Carlo Markov Chain search method for inverse modelling. At least 10^5 iterations were performed in a fixed time–temperature (t–T) frame ranging from 120 °C to 10 °C and from 250 Ma until present-day. The time–temperature path with the highest probability that gives the best fit with the fission track data is represented by the red path (i.e. maximum likelihood model) (Fig. 3). The black path (i.e. expected t–T model) is used for a more robust interpretation of the thermal history model (Gallagher, 2012) (Fig. 3).

A comparison between the traditional external detector method and the more recently developed LA-ICP-MS method (Hasebe et al., 2004) is made for one basement sample (AI-45). One apatite mount for this sample was etched in 5 M HNO_3 for 20.0 ± 0.5 s at 20.0 ± 0.5 °C to expose the spontaneous fission tracks and subsequently imaged on a Zeiss AXIO Imager M2m Autoscan System at the University of Adelaide. Fission track densities were measured using the FastTracks software and AFT ages were calculated using U concentrations, obtained simultaneously with the apatite U–Pb data acquisition. More details on the methodology are described in Gleadow et al. (2015), Gillespie et al. (2017), Glorie et al. (2017).

3.1.2. Detrital AFT dating application

In a sedimentary rock sample, different AFT age populations can be present because the sample possibly contains material originating from source terranes that experienced different t–T histories. The obtained single grain-age distributions for the detrital samples in this study are visualised by an abanico plot, which combines a radial plot with a Kernel Density Estimation (KDE) plot (Galbraith and Green, 1990), using the RadialPlotter software (Vermeesch, 2009). Central ages were calculated and a minimum age model was performed as well with the RadialPlotter software (Vermeesch, 2009). The homogeneity of the single-grain ages can be tested with a chi-squared test (χ^2; Galbraith, 1981; Green, 1981). If the sample passes the chi-squared test ($P(\chi^2) > 5\%$; Galbraith, 1981, Green, 1981), then it is assumed to be homogeneous; the single-grain ages belong to the same age group and the sample mean age is expressed by the central age. If the sample fails the chi-squared test ($P(\chi^2) < 5\%$; Galbraith 1981; Green 1981), then the sample possibly consists of a mixture of grains of different age populations. The spread of the single grain ages can also be evaluated by the age dispersion, i.e. for homogeneous populations of grain ages dispersion is normally <20% (Galbraith and Laslett, 1993). The obtained age components are compared with the cooling ages obtained for the hinterland and allow us to collect information on the provenance and the timing of exhumation-denudation in the adjacent basement sources. However, for detrital AFT dating, the provenance record can be (partially) erased (i.e. reset) by moderate levels (>2 km or >70 °C) of post-depositional burial-related heating (Green et al., 1989). As a possible indicator of this post-depositional annealing process, causing both age and confined track length reduction (Green et al., 1989), we have measured confined track lengths in the suitable samples in which a significant number of confined tracks could be measured. Track lengths were measured on 2000× magnification on a Nikon Eclipse NI-E microscope with a DS-Ri2 camera attached. Further on, we will link the new detrital AFT results to the detrital zircon U–Pb data from the same sedimentary sections (and where possible to the same samples) from De Pelsmaeker et al. (2018) to interpret the results. This multi-method approach enables an

Please cite this article in press as: Nachtergaele, S., et al., Meso-Cenozoic tectonic evolution of the Talas-Fergana region of the Kyrgyz Tien Shan revealed by low-temperature basement and detrital thermochronology, Geoscience Frontiers (2017), https://doi.org/10.1016/j.gsf.2017.11.007

evaluation of possible changes in provenance because the higher-temperature zircon U–Pb thermochronometer is insensitive to typical burial temperatures of sedimentary basins, specifically with respect to AFT annealing temperatures.

3.2. Zircon (U–Th)/He dating

Zircon (U–Th)/He (ZHe) dating is a low-temperature thermochronological method based on the temperature-dependent diffusion process of alpha, α particles (^{4}He), produced by alpha-decay of ^{238}U, ^{235}U and ^{232}Th in zircon. While He particles are expelled from the crystal lattice at high temperatures, they can remain trapped in the lattice at low temperatures. The mineral-specific Partial Retention Zone (PRZ) is the temperature window in which He is partially retained. The closure temperature (complete He retention) of the ZHe age system is ~175–195 °C for crystals of 40–100 μm in width that experienced a cooling rate of ~10 °C/Ma (Reiners et al., 2004). Hence, a ZHe age of a basement sample will be expected to be higher than its AFT age because the closure temperature of the AFT system is lower (see Section 3.1.1).

Four euhedral, inclusion-free zircons of two basement samples in close vicinity of the fault (AI-45 and KYR-05) with a minimum width of 75 μm were cleaned and wrapped separately in Nb tubes (Table 1, Fig. 2). These Nb tubes were heated and degassed, followed by the determination of ^{4}He concentration with isotope-dilution mass-spectrometry at the John de Laeter Center for Isotope Research at Curtin University (Perth, Australia). The determination of the U and Th concentrations was performed using isotope dilution ICP-MS. A detailed description of all analytical procedures can be found in Evans et al. (2005). The alpha ejection factor corrects the ZHe age for the amount of ^{4}He (α particles) that were ejected from the edges of the crystal due to the initial kinetic energy of the particles inherited from the α-disintegration reaction (Farley et al., 1996; Farley, 2002). The alpha ejection factor utilizes the geometry of the crystal and the assumption of an ideal, unbroken crystal morphology. Four different zircon crystal aliquots were analysed for each sample, because anomalously ZHe ages often need to be

Table 1
Sample locations, lithology, crystallisation or depositional age and methods used. AFT = Apatite Fission-Track dating, ZHe = Zircon (U–Th)/He dating, AUPb = Apatite U–Pb dating.

	Sample name	Latitude (°)	Longitude (°)	Alt. (m)	Location	Lithology	Crystallisation or depositional age	Method
Crystalline and Pre-Mesozoic basement samples	KB-121	N41.72575	E74.77587	2756	Song-Kul Tau Range	Syenite	Lower-Permian	AFT
	KB-122	N41.75243	E74.72218	2578	Song-Kul Tau Range	Metasandstone	Carboniferous	AFT
	KB-123	N41.8067	E74.6952	2431	Song-Kul Tau Range	Granodiorite	Upper-Ordovician	AFT
	KB-124	N41.83028	E74.68975	2385	Song-Kul Tau Range	Granodiorite	Upper-Ordovician	AFT
	KB-131	N41.72502	E74.53922	4143	Kavak-Tau Range	Granodiorite	Upper-Ordovician	AFT
	KB-132	N41.72625	E74.53442	3802	Kavak-Tau Range	Granodiorite	Upper-Ordovician	AFT
	KB-133	N41.72053	E74.5166	3387	Kavak-Tau Range	Granodiorite	Upper-Ordovician	AFT
	KB-134	N41.70848	E74.50908	2980	Kavak-Tau Range	Granodiorite	Upper-Ordovician	AFT
	KB-135	N41.70342	E74.50562	2822	Kavak-Tau Range	Granodiorite	Upper-Ordovician	AFT
	TF-06	N42.009167	E72.860556	1355	Talas Range, Chickhan	Granodiorite	Upper-Ordovician	AFT
	TF-15	N42.277222	E73.185833	3300	Talas Range, Ötmek	Granoditorite	Upper-Ordovician	AFT
	TF-16	N42.221944	E73.221111	2970	Talas Range, Ötmek	Granodiorite	Upper-Ordovician	AFT
	TF-23	N42.111667	E74.101667	2270	Djumgol Range, Kozjomkul	Granite	Upper-Ordovician	AFT
	KYR-02	N42.317778	E73.828056	2920	Kyrgyz range, Tuz-Asuu	Granite	Upper-Ordovician	AFT
	KYR-04	N41.711667	E72.943333	1625	Fergana Range, Toktogul	Mylonite	Proterozoic	AFT
	KYR-05	N41.722222	E72.968056	2110	Fergana Range, Toktogul	Metagranite	Proterozoic	AFT, ZHe
	KYR-15	N41.338056	E73.646944	2030	Fergana Range, Kazarman	Granodiorite	Carboniferous	AFT
	AI-44	N41.303611	E73.649444	2817	Fergana Range, Kaldama	Mylonite	Carboniferous	AFT
	AI-45	N41.346667	E73.663611	2125	Fergana Range, Urumbash	Granite	Carboniferous	AFT, ZHe, AUPb
	F11-775	N40.317222	E72.631667	1200	Kichi-Ali Range, Aral	Plagiogranite	Carboniferous	AFT
Jurassic –Paleogene detrital samples	KS13-01	N40.5245724	E73.4660265	1898	Fergana Basin (Jetim-Dobo)	Medium-grained sandstone	Jurassic-Cretaceous transition	AFT
	KS13-02	N40.5251986	E73.46581	1905	Fergana Basin (Jetim-Dobo)	Fine-grained sandstone	Jurassic-Cretaceous transition	AFT
	KS13-04	N40.5265722	E73.4697812	1910	Fergana Basin (Jetim-Dobo)	Medium-grained sandstone	Cretaceous	AFT
	KS13-08	N40.5312204	E73.4813711	1928	Fergana Basin (Jetim-Dobo)	Medium-grained sandstone	Cretaceous	AFT
	KS13-10	N40.5323412	E73.4501626	2328	Fergana Basin (Jetim-Dobo)	Medium-grained sandstone	Paleogene	AFT
	KS13-11	N41.3428186	E72.190518	658	Fergana Basin (Tash-Komyr)	Medium-grained sandstone	Jurassic	AFT
	KS13-13	N41.3375542	E72.1615515	777	Fergana Basin (Tash-Komyr)	Coarse-grained sandstone	Jurassic-Cretaceous transition	AFT
	KS13-16	N41.328087	E72.1694956	664	Fergana Basin (Tash-Komyr)	Coarse-grained sandstone	Paleogene	AFT
	KS13-17	N41.3264251	E72.169699	648	Fergana Basin (Tash-Komyr)	Coarse-grained sandstone	Paleogene	AFT
	KS13-18	N41.3258352	E72.1697056	636	Fergana Basin (Tash-Komyr)	Fine-grained sandstone	Paleogene	AFT
	KS13-19A	N40.8343698	E73.611686	1375	Yarkand-Fergana Basin (Yassy river)	Fine-grained sandstone	Jurassic-Cretaceous transition	AFT
	KS13-20	N40.8334599	E73.6098856	1370	Yarkand-Fergana Basin (Yassy river)	Medium-grained sandstone	Jurassic-Cretaceous transition	AFT
	KS13-22	N40.8450761	E74.0998915	2501	Yarkand-Fergana Basin (Chitty river)	Fine-grained sandstone	Jurassic	AFT
	KS-106	N40.40022	E74.36488	2992	Yarkand-Fergana Basin (Terek)	Medium-grained sandstone	Jurassic	AFT
	KS-113	N40.37615	E74.34135	2651	Yarkand-Fergana Basin (Terek)	Medium-grained sandstone	Cretaceous	AFT
	KS-126	N41.674972	E74.50725	2200	Ming-Kush-Kökömeren Basin (Ming-Kush)	Medium-grained sandstone	Jurassic	AFT
	KS-128	N41.67625	E74.507222	2280	Ming-Kush-Kökömeren Basin (Ming-Kush)	Coarse-grained sandstone	Jurassic	AFT

Please cite this article in press as: Nachtergaele, S., et al., Meso-Cenozoic tectonic evolution of the Talas-Fergana region of the Kyrgyz Tien Shan revealed by low-temperature basement and detrital thermochronology, Geoscience Frontiers (2017), https://doi.org/10.1016/j.gsf.2017.11.007

discarded due to tiny alpha-emitting micro-inclusions (e.g. monazite) and/or He trapping in radiation damaged zones of the crystal lattice (Reiners et al., 2004).

3.3. Apatite U–Pb dating

The apatite U–Pb (AUPb) dating method is based on temperature dependent diffusion of Pb in apatite and has a closure temperature (T_c) of ~350–550 °C (Chew and Spikings, 2015). Hence, AUPb is a medium to high temperature thermochronometric technique, whereas the aforementioned AFT (T_c ~ 100 °C), and ZHe (T_c ~175–195 °C) technique define the low temperature thermochronology. Apatite grains for one sample (AI-45) were analysed for U and Pb isotopes in the University of Adelaide using a New Wave UP213 laser connected to an Agilent-7900 ICP-MS, using similar settings as in Glorie et al. (2017). Calibrations and data reduction were conducted using Madagascar apatite as primary standard (ID-TIMS U–Pb age of 473.5 ± 0.7 Ma; Chew et al., 2014). McClure apatite (TIMS U–Pb age of 523.51 ± 1.47 Ma; Schoene and Bowring, 2006) and Durango apatite ($^{40}Ar/^{39}Ar$ age of 31.44 ± 0.18 Ma; McDowell et al., 2005) were used as secondary standards for accuracy checks. Data reduction was performed using the Iolite software (Paton et al., 2011) following the procedures described in Chew et al. (2014). A ^{207}Pb corrected overall weighted mean $^{238}U/^{206}Pb$ age was calculated, which represents the best estimate of the apatite U–Pb cooling age. More details on the methodology can be found in Chew et al. (2011, 2014).

4. Results

4.1. Basement thermochronology: AFT, ZHe and apatite U–Pb results

The apparent AFT ages of the twenty basement samples range from early Cretaceous to early Eocene and can be interpreted in terms of episodic basement cooling and protracted residence in the apatite Partial Annealing Zone (Figs. 2 and 3; Table 2). Fourteen Ordovician-Silurian granitoid samples and one Carboniferous meta-sandstone (KB-122) from in the NTS, four Carboniferous–Early Permian granitoid samples from the MTS and one Carboniferous–Early Permian granite from in the Alai Range in the STS (Fig. 2; Table 1) were analysed. All basement samples pass the chi-squared test (>5%) (Table 2). In total, 12 thermal history models are reconstructed using the QTQt software (Gallagher, 2012) based on samples with a sufficient to acceptable number of horizontal confined tracks (Fig. 3; Table 2).

The five samples (KB-131 to KB-135) from the Kavak-Tau Range (Fig. 2), north of the town of Ming-Kush, fit in a vertical profile ranging from 2800 to 4100 m in altitude and exhibit AFT ages ranging from the Early Cretaceous, 134.6 ± 6.5 Ma (KB-131) to the early Paleogene, 53.5 ± 3.0 Ma (KB-135). These samples yield relatively low mean track lengths between 11.8 and 12.7 μm, typical for undisturbed slowly cooled basement rocks (Gleadow et al., 1986) (Fig. 3, Table 2). The (three-phased) thermal history models of KB-131 – KB-134 indicate continuous Cretaceous basement cooling, followed by a very slow cooling or even stagnation during the Paleogene (Fig. 3). Cooling to ambient temperatures eventually transpired since the Neogene, although some model artefact could overestimate this.

The horizontal profile between Ming-Kush and Song Kul lake (KB-121 – KB-124; Fig. 2) shows AFT ages from the earliest Cretaceous (145.4 ± 9.5 Ma) to the Late Cretaceous (80.2 ± 5.6 Ma) (Table 2). These four samples have relatively low mean track lengths between 12.0 and 12.7 μm (Table 2). Thermal history models of KB 121-124 exhibit a comparable three-phased evolution as for the vertical sampling profile (KB-131–KB-135) (Fig. 3). Four additional samples from the western NTS (TF-15, TF-16, TF-23 and KYR-02) show Cretaceous AFT ages ranging from 115 to 100 Ma and relatively low mean track lengths of 11.7–12.8 μm. TF-06 is located north of the Toktogul lake (Fig. 2) and yields an Eocene AFT cooling age. Its thermal history model is only based on 43 confined track

Table 2
Basement apatite fission track analysis results. n is the number of counted apatite grains. ρ_s and ρ_i correspond to the density of spontaneous tracks (in the apatite) and induced tracks (in the muscovite external detector, ED) respectively. ρ_d-values are interpolated values of the density of induced tracks in the ED irradiated against regularly spaced Uranium-doped dosimeters (IRMM-540) in the irradiation package. ρ_s, ρ_i and ρ_d are expressed as 10^5 tracks/cm^2. N_s and N_i are the number of counted spontaneous tracks (in the apatite) and induced tracks (in the ED) respectively. N_d is the interpolated value of the number of counted induced tracks in the ED irradiated against the same glasses. P(χ^2) is the chi-squared probability that the dated grains have a constant ρ_s/ρ_i-ratio. AFT ages are reported as zeta-age $t(\zeta)$ (in Ma), calculated with the zeta calibration factor that is based on Durango and Fish Canyon Tuff age standard analyses. AFT length results are reported as mean track length (l_m in μm) with standard deviation σ (in μm), obtained from the measurement of an amount (n_l) of natural, horizontal confined tracks. For some samples, no AFT length data is reported due to low spontaneous track densities and/or a low number of suitable grains. Length data and subsequent thermal history modelling of samples in italic are based on low amounts of measured tracks and should be treated with caution. The AFT analyst is indicated in the last column (A), with DG (J. De Grave, ζ = 253.1 ± 2.4), GL (S. Glorie, ζ = 259.1 ± 3.3) and NA (S. Nachtergaele, ζ = 286.2 ± 4.7).

Sample	n	ρ_s (±1σ)	N_s	ρ_i (±1σ)	N_i	ρ_d (±1σ)	N_d	ρ_s/ρ_i (±1σ)	P(χ^2)	$t(\zeta)$	l_m	n_l	σ	A
TF-06	20	10.041 (0.315)	1014	10.612 (0.325)	1064	4.284 (0.101)	1791	0.972 ± 0.043	0.79	53.2 ± 2.8	12.8	43	1.1	GL
TF-15	20	15.451 (0.430)	1292	6.170 (0.277)	495	3.658 (0.076)	2323	2.520 ± 0.133	>0.99	115.6 ± 6.6	12.7	100	1.9	DG
TF-16	7	5.261 (0.592)	79	2.427 (0.405)	36	3.654 (0.076)	2316	2.228 ± 0.448	>0.99	102.2 ± 20.7	–	–	–	DG
TF-23	20	32.741 (0.671)	2384	17.358 (0.489)	1261	3.987 (0.096)	1727	1.940 ± 0.068	0.58	101.5 ± 4.5	12.2	100	1.6	GL
KYR-02	20	18.260 (0.577)	1001	9.294 (0.415)	501	4.158 (0.099)	1775	2.081 ± 0.114	0.54	115.5 ± 7.1	11.7	*30*	1.3	GL
KYR-04	30	7.099 (0.407)	304	3.812 (0.302)	159	3.102 (0.072)	1855	1.882 ± 0.184	1.00	73.5 ± 7.4	–	–	–	DG
KYR-05	25	10.222 (0.352)	843	4.232 (0.229)	341	3.113 (0.072)	1861	2.495 ± 0.160	0.91	97.5 ± 6.7	–	–	–	DG
KYR-15	11	18.302 (0.732)	626	8.618 (0.510)	286	4.118 (0.080)	2635	2.131 ± 0.152	0.60	110.1 ± 8.2	–	–	–	DG
AI-44	20	20.520 (0.480)	1827	9.287 (0.325)	819	4.128 (0.080)	2642	2.281 ± 0.096	0.98	118.1 ± 5.6	13.5	100	1.2	DG
AI-45	30	16.970 (0.375)	2048	9.047 (0.273)	1095	4.818 (0.098)	2409	1.905 ± 0.071	0.68	130.0 ± 5.8	12.8	100	1.5	NA
F11-775	20	21.528 (0.600)	1286	9.461 (0.399)	560	4.104 (0.080)	2628	2.295 ± 0.116	0.94	118.1 ± 6.5	13.2	100	1.5	DG
KB 121	20	5.296 (0.224)	555	3.936 (0.193)	414	4.046 (0.082)	2340	1.394 ± 0.091	0.98	80.2 ± 5.6	12.0	*30*	1.7	NA
KB 122	20	9.659 (0.307)	989	3.867 (0.194)	394	4.043 (0.082)	2324	2.542 ± 0.151	0.99	145.4 ± 9.5	12.7	100	1.2	NA
KB 123	20	6.063 (0.277)	479	3.527 (0.210)	280	4.027 (0.083)	2245	1.772 ± 0.133	0.99	101.3 ± 8.1	12.5	49	1.3	NA
KB 124	20	8.561 (0.316)	731	4.627 (0.232)	398	4.024 (0.084)	2230	1.956 ± 0.122	0.92	111.7 ± 7.5	12.5	*33*	1.3	NA
KB 131	20	15.781 (0.351)	2020	6.758 (0.229)	865	4.021 (0.084)	2217	2.358 ± 0.096	0.95	134.6 ± 6.5	12.6	75	1.3	NA
KB 132	20	14.932 (0.338)	1941	7.662 (0.242)	998	4.018 (0.084)	2204	1.986 ± 0.077	0.74	113.2 ± 5.3	12.7	100	1.2	NA
KB 133	20	13.997 (0.342)	1666	8.208 (0.262)	978	4.016 (0.084)	2190	1.730 ± 0.070	0.32	98.6 ± 4.8	12.3	100	1.2	NA
KB 134	20	10.706 (0.293)	1331	9.782 (0.281)	1211	4.013 (0.084)	2177	1.121 ± 0.045	0.88	64.1 ± 3.1	11.8	69	1.8	NA
KB 135	20	6.219 (0.223)	777	6.698 (0.231)	837	4.010 (0.084)	2162	0.936 ± 0.047	0.78	53.5 ± 3.0	13.0	*20*	1.6	NA

Please cite this article in press as: Nachtergaele, S., et al., Meso-Cenozoic tectonic evolution of the Talas-Fergana region of the Kyrgyz Tien Shan revealed by low-temperature basement and detrital thermochronology, Geoscience Frontiers (2017), https://doi.org/10.1016/j.gsf.2017.11.007

Table 3
Zircon (U–Th)/He analysis results. For each sample, four single grain ages (aliquots) were determined. Analyses in italic were discarded for the calculation of the sample's average age, because of anomalous values possibly caused by inclusions or Helium trapping in the zircon crystals (see Section 3.2). Ft is the alpha-ejection parameter as defined by Farley et al. (1996). Uncorrected ages (Unc. age) are corrected (Cor. age) based on the Ft correction factor. TAU is the Total Analytical Uncertainty.

Sample	U (ppm)	σ	Th (ppm)	σ	He (ncc)	He err (%)	TAU (%)	Th/U	Unc. age (Ma)	σ	Ft	Cor. Age (Ma)	σ	Average (Ma)
AI-45 1	*979.3*	*19.5*	*1444.1*	*28*	*260.6*	*2.5*	*3*	*1.5*	*340.37*	*10.08*	*0.77*	*443.32*	*13.85*	160.3 ± 5.3
AI-45 2	1160	27.2	1449.5	21.1	91.1	2.5	3.1	1.2	119.48	3.73	0.76	157.69	5.84	
AI-45 3	768.6	16.4	377.2	7.3	59.3	2.6	3.2	0.5	131.21	4.19	0.76	171.91	6.48	
AI-45 4	1068.9	28.4	887	12.9	130.9	2.5	3.4	0.8	121.39	4.08	0.8	151.15	5.31	
KYR05-1	*254*	*5.8*	*315.7*	*6.2*	*10.5*	*2.6*	*3.1*	*1.2*	*160.91*	*5.07*	*0.69*	*231.76*	*8.65*	155.4 ± 6.0
KYR05-2	427.3	9.1	428.5	8.4	5.1	1.7	2.4	1	73.99	1.8	0.61	120.35	4.65	
KYR05-3	564.1	12	565.6	11.1	6.2	1.5	2.3	1	90.21	2.07	0.61	148.95	5.62	
KYR05-4	649.3	16.5	342.3	7.2	8.6	1.3	2.6	0.5	120.27	3.17	0.61	196.79	7.86	

lengths and therefore not used for in depth discussion, but shows analogies with KB-134 from the vertical profile.

Samples KYR-04, KYR-05, KYR-15, AI-44 and AI-45 originate from several basement blocks located inside or in close proximity of the TFF (Fig. 2). The samples from the Kazarman pass site (KYR-15, AI-44 and AI-45) yield AFT ages from 130 to 110 Ma (Table 2). Younger, Cretaceous AFT ages of ~100–70 Ma are obtained on the TFF segment south of the Toktogul lake in samples KYR-04 and KYR-05 (Fig. 2; Table 2). LA-ICP-MS based AFT analysis on AI-45 determined a central age of 132.0 ± 5.2 Ma, based on 23 apatite grains. This central age is, within 1σ uncertainty, similar to the central age that has been obtained with the external detector method (127.7 ± 4.8 Ma).

ZHe dating (T_c ~175–195 °C) for two of these basement samples from faulted blocks close to the TFF, AI-45 and KYR-05, yield Late Jurassic mean ages of 160.3 ± 5.3 Ma and 155.4 ± 6.0 Ma respectively (Table 3). For both AI-45 and KYR-05, one anomalously old single grain ZHe age was excluded in the calculation of the mean ZHe age. The anomalously high age could possibly be related to alpha-emitting mineral micro-inclusions (e.g. monazite) or He-trapping due to radiation damage in the zircon crystal (Guenther et al., 2013) (Table 3). The mean ZHe age based on three out of four aliquots is for both samples older than their corresponding AFT age of 127.7 ± 4.8 Ma and 97.5 ± 6.7 Ma respectively (Tables 2 and 3). The three ZHe single grain ages, the AFT ages and track length information and the apatite U–Pb age (see next paragraph) were used for thermal history modelling of sample AI-45. A radiation damage model (Guenther et al., 2013) appropriate for zircon was incorporated in the thermal history model of AI-45. The well-constrained thermal history model and moderately high mean track length of AI-45 indicate rapid cooling trough the APAZ around ~130–120 Ma (Fig. 3).

A ^{207}Pb corrected overall weighted mean apatite ^{238}U/^{206}Pb age (T_c ~350–550 °C) of 285.8 ± 4.1 Ma was obtained for AI-45. Uranium concentrations ranged from 11.82 to 52.00 ppm in the 22 analysed apatite grains. The concordia diagram and the weighted mean age plot can be found in the supplementary material. The ^{207}Pb corrected overall weighted mean apatite ^{238}U/^{206}Pb age of 285.8 ± 4.1 Ma for AI-45 is consistent with earlier published data of Late Paleozoic post-collisional intrusives with zircon U–Pb ages of 290–275 Ma (Seltmann et al., 2011). These deformed intrusives exhibit Permo-Triassic to Early Jurassic ^{40}Ar–^{39}Ar ages obtained on synkinematic muscovite (T_c ~ 400 ± 50 °C) and biotite (T_c ~ 335 ± 50 °C) (Harrison et al., 1985; Konopelko et al., 2013; Rolland et al., 2013).

Geographically isolated sample F11-775 originates from the Alai Range, west of the TFF in the STS, and has an Early Cretaceous AFT age of 118.1 ± 6.5 Ma and a relatively high mean track length of 13.2 μm (Figs. 2 and 3). The well-constrained thermal history model of F11-775 indicates cooling since the Cretaceous (Fig. 3).

4.2. Detrital apatite fission track results

4.2.1. Ming-Kush-Kökömeren Basin

The Ming-Kush sedimentary section is located to the east of the TFF, in the narrow transpressive Ming-Kush-Kökömeren Basin, west of the Song-Kul plateau and close to the Nikolaev line (Fig. 2). The analysed Jurassic sandstones fit in high-resolution sedimentary logs of the Jurassic and early Paleogene sediments (De Pelsmaeker et al., 2018), exposed just north of the town of Ming-Kush. The maximum thickness in the Ming-Kush-Kökömeren Basin of the Jurassic sediments is 680 m and the overlying Paleogene-Neogene sediments do not exceed 2 km (Bachmanov et al., 2008). Samples KS-126 and KS-128, with an Early to Middle Jurassic stratigraphic age (~200–160 Ma) based on plant fossils (Bachmanov et al., 2008), yield central detrital AFT ages of 198 ± 16 Ma (n_c = 7 and P(χ^2) = 0.76) and 202.9 ± 9.2 Ma (n_c = 37 and P(χ^2) = 0.99), respectively (Table 4, Fig. 4). For both samples, the central age is hence slightly older than their corresponding stratigraphic age. KS-126 and KS-128 yield relatively high mean track lengths of 13.5 μm (with a narrow distribution, moderate to low standard deviation of 1.6 μm) and 13.3 μm (with a narrow distribution, moderate to low standard deviation of 1.3 μm), based on 29 and 133 confined track length measurements respectively (Fig. 5, Table 4). Therefore, it can be assumed that the AFT ages have not (or only slightly) been reset and that they reflect inherited AFT cooling age populations from the source areas (Figs. 4 and 6).

4.2.2. Fergana Basin

The other three sedimentary sections are located west of the TFF, one in the Yarkand-Fergana (section 4.2.3) and two in the Fergana basin (Fig. 2). The two sedimentary sections of the Fergana Basin were studied close to the villages of Tash-Komyr and Jetim-Dobo respectively. For each section, five Jurassic–Paleogene samples were analysed (Figs. 2 and 4; Tables 1 and 4). The *Tash-Komyr section* is located in the northeastern part of the Fergana Basin and includes Jurassic, Cretaceous to early Paleogene sediments (Fig. 2). The total thickness of the Meso- and Cenozoic sediments is estimated at 2400 m at the Tash-Komyr section, based on the findings of De Pelsmaeker et al. (2018) and Bande et al. (2015a). The detrital apatites from the Middle–Upper Jurassic samples KS13-11 (n_c = 51) and KS13-13 (n_c = 39) yield central ages of 118 ± 11 Ma (n_c = 51 and P(χ^2) = 0.33) and 121.8 ± 7.8 Ma (n_c = 39 and P(χ^2) = 0.67). These Early Cretaceous ages are obviously younger than their corresponding stratigraphic age (Figs. 4 and 6; Table 4), suggesting that the AFT system of these samples experienced a certain degree of partial resetting, due to post-depositional burial reheating. Three Paleogene samples (KS13-16, KS13-17 and KS13-18) were also analysed. From those, only less than 20 apatite crystals could be analysed for each sample (Table 4). KS13-16 is sampled just below the marine Ypresian-Bartonian (Eocene) limestones (Bosboom et al., 2015) and KS13-17 and KS13-18 were sampled in between

Please cite this article in press as: Nachtergaele, S., et al., Meso-Cenozoic tectonic evolution of the Talas-Fergana region of the Kyrgyz Tien Shan revealed by low-temperature basement and detrital thermochronology, Geoscience Frontiers (2017), https://doi.org/10.1016/j.gsf.2017.11.007

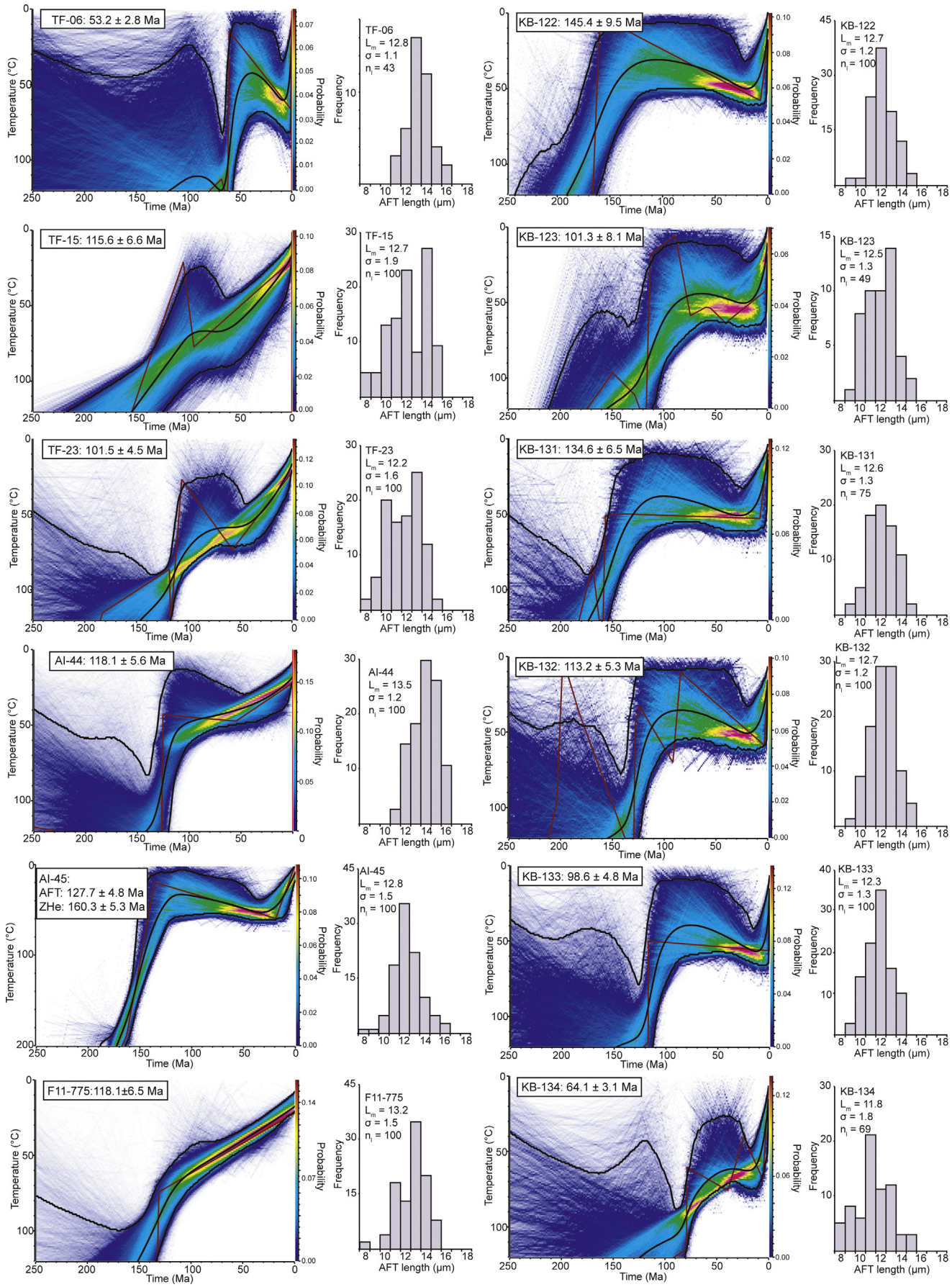

Please cite this article in press as: Nachtergaele, S., et al., Meso-Cenozoic tectonic evolution of the Talas-Fergana region of the Kyrgyz Tien Shan revealed by low-temperature basement and detrital thermochronology, Geoscience Frontiers (2017), https://doi.org/10.1016/j.gsf.2017.11.007

these Ypresian-Bartonian limestone layers (De Pelsmaeker et al., 2018). Given (1) the low number of available apatite crystals for each of the samples, (2) the small range in stratigraphic age and (3) their similar detrital zircon U–Pb signal (indicating similar source areas, De Pelsmaeker et al., 2018), the three samples are displayed on a single pooled radial plot (Fig. 4). The single-grain detrital AFT ages obtained for these three samples are all older than the stratigraphic age (which is ~40–55 Ma), and the central age for the pooled Paleogene samples is 104.5 ± 8.9 Ma (n = 27 and $P(\chi^2) < 0.05$; Fig. 4; Table 4). Therefore, it is assumed that these samples are not affected by significant post-depositional reheating and preserve their inherited AFT age components.

The *Jetim-Dobo section* is located in the southeastern Fergana Basin, and includes Jurassic, Cretaceous and early Paleogene sediments (Fig. 2; De Pelsmaeker et al., 2018). KS13-01 and KS13-02 were sampled at the Jurassic – Cretaceous transition and yield central ages of 144.0 ± 4.8 Ma (n_c = 84 and $P(\chi^2) = 0.11$) and 148.4 ± 8.3 Ma (n_c = 51 and $P(\chi^2) = 0.92$), which, within uncertainty, compares to their stratigraphic age (Figs. 4 and 6; Table 4). The mean track length of KS13-01 of 11.6 μm with a narrow distribution (SD = 1.4 μm), is based on 289 horizontal confined track length measurements (Fig. 5; Table 4). Considering that both samples contain both older and younger single grain AFT ages with respect to their stratigraphic age, we can conclude that they experienced at least some burial reheating between ca. 2 and 4 km depth without complete resetting and that the central ages thus represent mixed ages. Higher up in the stratigraphy, a Lower Cretaceous sandstone sample KS13-04 yields a central age of 123.8 ± 6.1 Ma (n_c = 90 and $P(\chi^2) = 0.81$) and an Upper Cretaceous sample KS13-08 yields a central age of 130.4 ± 5.3 Ma (n_c = 76 and $P(\chi^2) < 0.05$). The mean track length of sample KS13-08 equals 12.1 μm (n_l = 392 with SD = 1.4 μm). Paleogene sample KS13-10 is located just below the Eocene limestones and yields a central age of 84.1 ± 3.9 Ma (n_c = 57 and $P(\chi^2) = 0.00$). The mean track length (l_m = 11.9 μm with SD = 1.1 μm; n_l = 62) of this sample is very similar to the two samples located lower in the stratigraphy. The Upper Cretaceous and Lower Paleogene samples all contain single grain AFT ages which are older or comparable in age with respect to the stratigraphic age. Therefore, it can be assumed that the Upper Cretaceous and Paleogene layers have not experienced significant thermal resetting and preserved all or most inherited AFT information.

4.2.3. Yarkand-Fergana Basin

The *Yarkand-Fergana Basin* is located just to the southwest of the TFF and likely formed during an Early–Middle Jurassic regional transtensional regime in which the TFF played a major role (Burtman, 1980; Sobel, 1999; Alexeiev et al., 2017). The basin contains a remarkable thick (>3 km) succession of Jurassic sediments close to the fault, which taper out and become thinner away from the fault. From the Yarkand-Fergana Basin, five Jurassic–Cretaceous samples were analysed: two samples (KS-106 and KS-113) from the Terek section in the central part of the basin and three samples (KS13-19, KS13-20, and KS13-22) were sampled in incised river valleys in the northern part of the basin (Fig. 2; Tables 1 and 4). The ca. 2700 m thick Terek stratigraphic section includes the Middle Jurassic and a large part of the Cretaceous (De Pelsmaeker et al., 2018). The Middle Jurassic sample KS-106 was taken ca. 50 m above the Palaeozoic basement contact and yields a central age of 25.1 ± 1.8 Ma (n_c = 82 and $P(\chi^2) < 0.05$). These data can be interpreted in terms of significant to total track annealing (Figs. 4 and 6; Table 4). Cretaceous sample KS-113 is located 2000 m higher in the stratigraphic column and yields a central age of 61.1 ± 2.9 Ma (n_c = 105 and $P(\chi^2) < 0.05$). From the radial plot it is clear that the sample contains a mix of older and younger single grain AFT ages in respect to its stratigraphic age and can therefore be interpreted as partially reset (Fig. 4). The Middle–Upper Jurassic sample KS13-22 is sampled in close proximity of the TFF (Fig. 2). A central age of 11.4 ± 0.9 Ma (n_c = 35 and $P(\chi^2) < 0.05$) is obtained and all single grain AFT ages are clearly younger than the stratigraphic age (Fig. 4; Table 4). The sample can therefore be interpreted as totally reset. KS13-19 and KS13-20 are sampled at the bottom of the Kyrgyz equivalent (De Pelsmaeker et al., 2018) of the Kalaza conglomerate formation of the Chinese Tien Shan (stratigraphic age of ca. 145 Ma; Jolivet et al., 2015), and yield central ages of 110 ± 6.1 Ma (n_c = 38 and $P(\chi^2) = 0.98$) and 102.2 ± 6.3 Ma (n_c = 31 and $P(\chi^2) = 1.00$), respectively, again significantly younger than their stratigraphic age. The latter two samples show a significant to total degree of track annealing because they contain a mixture of older and younger single grain AFT ages with respect to their stratigraphic age (Fig. 4).

5. Discussion

In the following, we interpret our thermochronological results in terms of the Meso-Cenozoic tectonic evolution and associated basement cooling of the Kyrgyz Tien Shan, their denudation and sediment accumulation in developing intramontane basins.

5.1. Basement thermochronological data

The ZHe ages of samples AI-45 and KYR-05 (~160–155 Ma) located in the TFF zone demonstrate that the TFF was active in the early Late Jurassic (Oxfordian). Fault movements and associated potential hydrothermal activity channelled in the fault induced temperature high enough to reset the ZHe system. These results are in agreement with the Early–Middle Jurassic $^{40}Ar/^{39}Ar$ ages obtained on deformed synkinematic mica of the same region (Rolland et al., 2013).

New basement AFT ages (145–53 Ma) span most of the Cretaceous–early Paleogene period, with the most abundant AFT ages between 130 and 100 Ma (Table 2). Twelve samples in the NTS and MTS at the eastern side of the TFF (KB-123, KB-124, KB-132, KB-133, TF-15, TF-16, TF-23, KYR-02, KYR-05, KYR-15, AI-44, AI-45), and one sample (F11-775) from the Alai region at the western side yield such AFT ages (130–100 Ma) (Fig. 2; Table 2). The mean track length for the samples with ages between 130 and 100 Ma is between 13.5 and 12.2 μm, while the mean track length tends to decrease (and the standard deviation increases) for samples with AFT ages ranging from 100 to 65 Ma (TF-23, KB-133 and KB-134), as displayed on the "boomerang-shaped" age vs. mean track length plot (Green et al., 1986) of Fig. 7. So, on Fig. 7, only the half boomerang is exposed, giving us the signature of an exhumed fossil APAZ with an Early Cretaceous exhumation event (high AFT age vs. high mean track length) with a tail of mixed signature (the APAZ shortening) with AFT ages from the Late Cretaceous to Early Paleogene and

Figure 3. Thermal history models are reconstructed using the QTQt software (Gallagher, 2012) and the (Ketcham et al., 2007) algorithm and are applied to crystalline basement samples with a sufficient to acceptable number of measureable horizontal confined tracks (Table 2). AFT length data is displayed with each thermal history model. The colour scale indicates high probability in red and yellow, and the blue colours indicate lower probability values. The central black curve and its surrounding envelope display the expected time-temperature (t–T) model and the 95% probability range interval. The red line indicates the maximum likelihood model (Gallagher, 2012). A fixed time-temperature interval of (0–120 °C and 250–0 Ma) is maintained for every thermal history model. For each sample the AFT age is displayed, together with the mean length (l_m), standard deviation (σ) and number of track lengths (n_l).

Please cite this article in press as: Nachtergaele, S., et al., Meso-Cenozoic tectonic evolution of the Talas-Fergana region of the Kyrgyz Tien Shan revealed by low-temperature basement and detrital thermochronology, Geoscience Frontiers (2017), https://doi.org/10.1016/j.gsf.2017.11.007

Table 4
Detrital apatite fission track analysis results. The stratigraphic age of each sample is abbreviated (J. = Jurassic, Cr. = Cretaceous, Pg. = Paleogene). n_c is the number of counted grains. ρ_s and ρ_i correspond to the density of spontaneous tracks (in the apatite) and induced tracks (in the muscovite external detector, ED) respectively. ρ_d-values are interpolated values of the density of induced tracks in the ED irradiated against regularly spaced Uranium-doped glass dosimeters (IRMM-540) in the irradiation package. ρ_s and ρ_i are expressed as 10^6 tracks/cm^2. ρ_d is expressed as 10^5 tracks/cm^2. N_s and N_i are the number of counted spontaneous tracks (in the apatite) and induced tracks (in the ED) respectively. N_d is the interpolated value of the number of counted induced tracks in the ED attached to the same glasses during irradiation. P(χ^2) is the chi-squared probability that the dated grains have a constant ρ_s/ρ_i-ratio (Galbraith, 1981). The AFT central age t(c) (in Ma), age dispersion (%) and minimum age (Min. age) are calculated using the RadialPlotter software (Vermeesch, 2009). Mean track length (l_m), standard deviation (σ) and the number of track lengths (n_l) are measured for the highest quality samples in which it was possible to measure a significant number of horizontal confined tracks. AFT analyst is indicated in the last column (A), with DP (E. De Pelsmaeker, $\zeta = 264.2 \pm 4.1$) and NA (S. Nachtergaele, $\zeta = 286.2 \pm 4.7$).

Sample name	Dep. age	n_c	ρ_s ($\pm1\sigma$)	N_s	ρ_i ($\pm1\sigma$)	N_i	ρ_d ($\pm1\sigma$)	N_d	ρ_s/ρ_i ($\pm1\sigma$)	P(χ^2)	t (c) $\pm 1\sigma$ (Ma)	l_m	n_l	σ	Dpar	Age disp. (%)	Min. age (Ma)	A
Fergana Basin (Jetim-Dobo)																		
KS13-01	J.-Cr.	84	1.220 (0.021)	3514	0.613 (0.015)	1740	5.455 (0.092)	3491	2.148 (0.063)	0.11	144.0 ± 4.8	11.6	289	1.3	1.4	13	127 ± 19	DP
KS13-02	J.-Cr.	51	1.066 (0.033)	1035	0.546 (0.025)	496	5.469 (0.092)	3500	2.164 (0.118)	0.92	148.4 ± 8.3	–	–	–	–	7	72 ± 72	DP
KS13-04	Cr.	90	1.515 (0.042)	1320	0.876 (0.032)	766	5.426 (0.092)	3473	2.043 (0.093)	0.81	123.8 ± 6.1	–	–	–	–	16	105 ± 18	DP
KS13-08	Cr.	76	1.786 (0.024)	5832	0.914 (0.017)	2938	4.583 (0.085)	2934	2.186 (0.049)	0.00	130.4 ± 5.3	12.1	388	1.4	1.4	28	90.4 ± 6.2	NA
KS13-10	Pg.	57	0.966 (0.028)	1856	0.729 (0.019)	1459	4.558 (0.084)	2918	1.493 (0.052)	0.00	84.1 ± 3.9	11.9	62	1.1	1.3	18	65 ± 10	NA
Fergana Basin (Tash-Komyr)																		
KS13-11	J.	51	1.160 (0.055)	443	0.706 (0.042)	280	5.497 (0.093)	3518	2.162 (0.165)	0.33	118.0 ± 11	–	–	–	–	29	91 ± 31	DP
KS13-13	J.-Cr.	39	0.939 (0.033)	812	0.478 (0.023)	434	4.549 (0.084)	2912	2.318 (0.138)	0.67	121.8 ± 7.8	–	–	–	–	11	113 ± 20	NA
KS13-16	Pg.	6	0.647 (0.042)	240	0.487 (0.036)	181	4.544 (0.084)	2909	1.448 (0.143)	0.00	85.0 ± 16	–	–	–	–	36	60 ± 11	NA
KS13-17	Pg.	9	1.181 (0.101)	138	0.755 (0.077)	97	4.540 (0.084)	2907	1.506 (0.200)	0.51	91.0 ± 13	–	–	–	–	14	83 ± 31	NA
KS13-18	Pg.	12	1.550 (0.072)	470	0.835 (0.054)	237	4.535 (0.084)	2904	2.055 (0.164)	0.12	126.0 ± 13	–	–	–	–	20	99 ± 32	NA
Yarkand-Fergana Basin (Yassy river, Chitty river and Terek)																		
KS13-19A	J.-Cr.	38	1.003 (0.034)	885	0.564 (0.025)	515	4.513 (0.084)	2889	1.930 (0.107)	0.98	110.0 ± 6.1	–	–	–	–	0	109.3 ± 6.6	NA
KS13-20	J.-Cr.	31	1.099 (0.042)	677	0.669 (0.034)	424	4.508 (0.084)	2886	1.709 (0.106)	1.00	102.2 ± 6.3	–	–	–	–	0	101.2 ± 6.6	NA
KS13-22	J.	35	0.222 (0.013)	279	1.212 (0.034)	1595	4.504 (0.084)	2884	0.206 (0.013)	0.03	11.4 ± 0.9	–	–	–	–	25	9.5 ± 5.3	NA
KS-106	J.	82	0.304 (0.009)	1129	0.969 (0.016)	3904	5.392 (0.092)	3451	0.500 (0.017)	0.00	25.1 ± 1.8	–	–	–	–	50	13.7 ± 4.6	DP
KS-113	Cr.	105	0.704 (0.014)	2481	0.849 (0.016)	3005	5.409 (0.092)	3462	1.085 (0.029)	0.00	61.1 ± 2.9	–	–	–	–	35	38.7 ± 4.0	DP
Ming-Kush-Kökömeren Basin (Ming-Kush)																		
KS-126	J.	7	1.586 (0.063)	628	0.533 (0.037)	205	4.592 (0.085)	2940	2.828 (0.228)	0.76	198 ± 16	13.5	29	1.6	1.7	0	197 ± 17	NA
KS-128	J.	37	0.981 (0.022)	1997	0.311 (0.012)	636	4.587 (0.085)	2937	3.303 (0.150)	0.99	202.9 ± 9.2	13.3	133	1.3	1.8	0	200.7 ± 9.9	NA

lower track length values. This is also evident from the thermal history models (Fig. 3). Fig. 7 further suggests that the basement rocks of the NTS and MTS, with AFT ages from 130 to 100 Ma, cooled more rapid than the basement rocks of the NTS and MTS with AFT ages of 100–65 Ma. Comparable Late Jurassic – Cretaceous basement AFT ages are ubiquitously found in the NTS (Sobel et al., 2006b; Glorie et al., 2010; De Grave et al., 2011a, 2013; Macaulay et al., 2014; De Pelsmaeker et al., 2015), MTS (Glorie et al., 2011; Macaulay et al., 2014; Wang et al., 2017) and STS (Sobel et al., 2006a; De Grave et al., 2012; Käßner et al., 2016) (Figs. 2 and 5), but the AFT ages of 130–100 Ma seem to be more abundant in the Kyrgyz Tien Shan than the 100–65 Ma cooling ages (Glorie and De Grave, 2016), although sampling bias can also have an influence here. We speculate that the sampled basement rocks with AFT ages ranging from 100 to 65 Ma are affected by a prolonged residence in the APAZ and represent an uplifted/exhumed APAZ. Therefore these latter ages are less meaningful and postdate the actual event.

Some authors find young Cenozoic AFT (and zircon He) ages, mainly Oligocene and Neogene, in and along the TFF fault zone, corresponding to the timing of the most recent and ongoing tectonic reactivation of the Tien Shan orogenic edifice (e.g. Yang et al., 2014; Bande et al., 2015a,b, 2017 and references therein). They are mainly constrained to the horsetail structures at the northern (Chatkal ranges) and southern (Alai and Kokshaal ranges) ends of the TFF trace, but occur along the fault as well. This indicates that recent movements along the fault have induced basement exhumation as well. From the sampled basement blocks in this study, no such young ages were retrieved; as mentioned, the bulk of our basement samples yield Cretaceous AFT ages. For example, our sample AI-45, from a massive, un-sheared granite wall down the eastern flank of the Fergana Range (east of TFF, over the Kazarman and Kaldama passes down to Urumbash, Table 1) was analysed via different techniques. The sample was analysed by different operators (SN and SG), in different laboratories (Ghent and Adelaide), with different methods (traditional external detector and LA-ICP-MS respectively), and different etching conditions (5.5 M, 20 s, 21 °C, analyst SN and 5.0 M, 20 s, 20 °C, analyst SG). The obtained results for AI-45, using the different analytical protocols, confirm each other and render an Early Cretaceous AFT age (central AFT ages are 127.7 ± 4.8 Ma for the external detector method and 132.0 ± 5.2 Ma for the LA-ICP-MS based method). This sample was also analysed with the ZHe method as explained above, giving an average Late Jurassic age of ~160 Ma (Table 3). So for this area, a clear Late Jurassic–Early Cretaceous low-temperature thermochronometric signal is preserved.

5.2. Detrital AFT data and implications for burial depth

The Jurassic detrital sediment samples east (Ming-Kush-Kökömeren Basin) and west of the TFF (Yarkand-Fergana and Fergana basins) clearly exhibit different AFT central ages. The Jurassic sediments of the Ming-Kush-Kökömeren Basin (KS-128 and KS-126) with Triassic–Early Jurassic (~200 Ma) central AFT ages and high mean track lengths (~13.5 μm), indicate limited or no post-depositional burial resetting in this sample site. Hence, their ages reflect the inherited AFT age populations of the source areas. In the Jetim-Dobo section of the Fergana Basin, five sediment samples with depositional ages varying between the Jurassic-Cretaceous transition and early Paleogene show a gradual shift from partially reset (samples KS13-01, KS13-02, KS13-04 with AFT central ages ~148–124 Ma) towards non-reset (samples KS13-08 and KS13-10 with central AFT ages of ~130 Ma and 84 Ma respectively) AFT central ages (Figs. 4 and 6). The Jurassic–Cretaceous sample KS13-01 from Jetim-Dobo has a low mean track length of 11.6 μm, which is expected, since the sample is thought to be partially reset which indeed should result in annealing and track length shortening. Also in the Tash-Komyr section of the Fergana Basin a similar trend can be observed with partially reset AFT ages for the Jurassic–early Cretaceous samples KS13-11 and KS13-13 (AFT central ages of ~118 and 122 Ma respectively) towards non-reset AFT ages for the Paleogene samples (KS13-16/17/18 with central AFT age of ~105 Ma). In the Yarkand-Fergana Basin, five sedimentary samples with depositional ages between the Jurassic and the Cretaceous show a trend from even totally reset (samples KS13-22 and KS-106 with AFT central ages of ~11 Ma and ~25 Ma respectively) towards partially reset (samples KS13-19A, KS13-20, KS-113 with AFT central ages of ~110–60 Ma) AFT ages.

In general, the Jurassic samples of the Ming-Kush-Kökömeren Basin to the east of the TFF are not reset, or slightly at best, by post-depositional burial, while most Jurassic–Cretaceous samples of the Fergana and Yarkand Fergana basins to the west of the TFF are distinctively partially-to-totally reset. Hence, the AFT central ages of the latter samples represent mixed ages. From all the analysed samples west of the TFF, we assume that only the Upper Cretaceous sample KS13-08 from Jetim-Dobo and the Paleogene samples of both the Jetim-Dobo and Tash-Komyr sections from the Fergana Basin have not experienced significant post-depositional reheating and preserved their inherited AFT age signals from the source areas.

Paleogene sample KS13-10 of the Jetim Dobo section is mainly characterized by broadly distributed Cretaceous single grain detrital AFT ages, with a central age of 84.1 ± 3.9 Ma and mean track length of 11.9 μm. Just as KS13-08, this sample contains, Cretaceous single grain AFT ages with mean track lengths ~12.0 μm. It is most plausible that the track length data are “inherited” from the source region, since the Late Cretaceous apatite fission track data typically yields lengths ~12 μm (Fig. 7). But, it is not possible to exclude the influence of post-depositional reheating and associated track length shortening. Paleogene samples KS13-16, KS13-17 and KS13-18 express broadly distributed single grain data with a pooled central age of ~104.5 ± 8.9 Ma. It is not possible to draw any conclusions concerning age populations from this limited amount of single grain age data. Generally, Paleogene samples of the Fergana basin exhibit dispersed Cretaceous AFT single grain ages and show no clear signs of thermal resetting.

Since some Mesozoic samples experienced a different degree of thermal resetting through post-depositional burial, it is possible to draw preliminary conclusions concerning maximal burial depth. The Fergana basin is characterized by a continuous deposition of Mesozoic sediments from the Jurassic to the Cretaceous, while the Cretaceous sediments appear to be absent in the Ming-Kush-Kökömeren Basin. Based on the contrasting AFT central ages of the Jurassic samples on both sides of the TFF, we propose that the Meso-Cenozoic basins of the Kyrgyz Tien Shan experienced a different post-Jurassic burial history. In the Yarkand-Fergana Basins to the west of the TFF, sedimentary burial must have exceeded ~3–4 km deep to significantly to even totally resetting the AFT system, while sedimentary burial to the east of the TFF was less important and likely caused limited or no post-depositional burial resetting of the Jurassic sediments in Ming-Kush sample site.

Our findings are in good agreement with the study of Yang et al. (2014), in which Middle Jurassic and Lower Cretaceous sediment samples of the Chinese part of the Yarkand-Fergana Basin are also completely reset and show central ages of 18.5 ± 5.2 and 16.6 ± 2.8 Ma respectively, while the overlying Upper Cretaceous and Paleogene sediments are partially reset, and the Neogene sediments are not reset at all (Yang et al., 2014). Some Early Cretaceous ‘age components’ are also preserved in two not-to-poorly reset Cretaceous samples from the southwestern Chinese Tien Shan (Yang et al., 2014). Cretaceous ages are also reported in

Please cite this article in press as: Nachtergaele, S., et al., Meso-Cenozoic tectonic evolution of the Talas-Fergana region of the Kyrgyz Tien Shan revealed by low-temperature basement and detrital thermochronology, Geoscience Frontiers (2017), https://doi.org/10.1016/j.gsf.2017.11.007

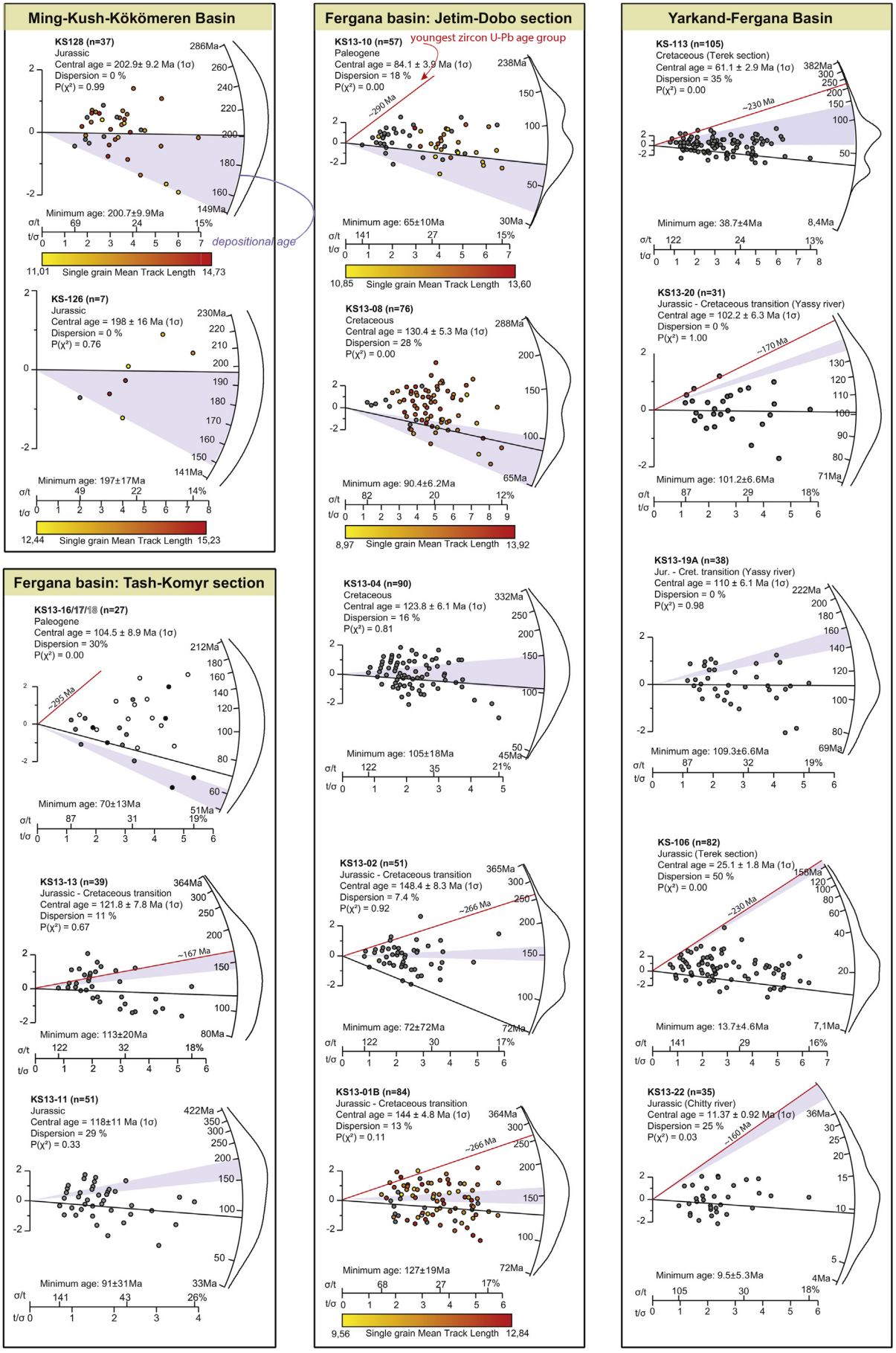

Please cite this article in press as: Nachtergaele, S., et al., Meso-Cenozoic tectonic evolution of the Talas-Fergana region of the Kyrgyz Tien Shan revealed by low-temperature basement and detrital thermochronology, Geoscience Frontiers (2017), https://doi.org/10.1016/j.gsf.2017.11.007

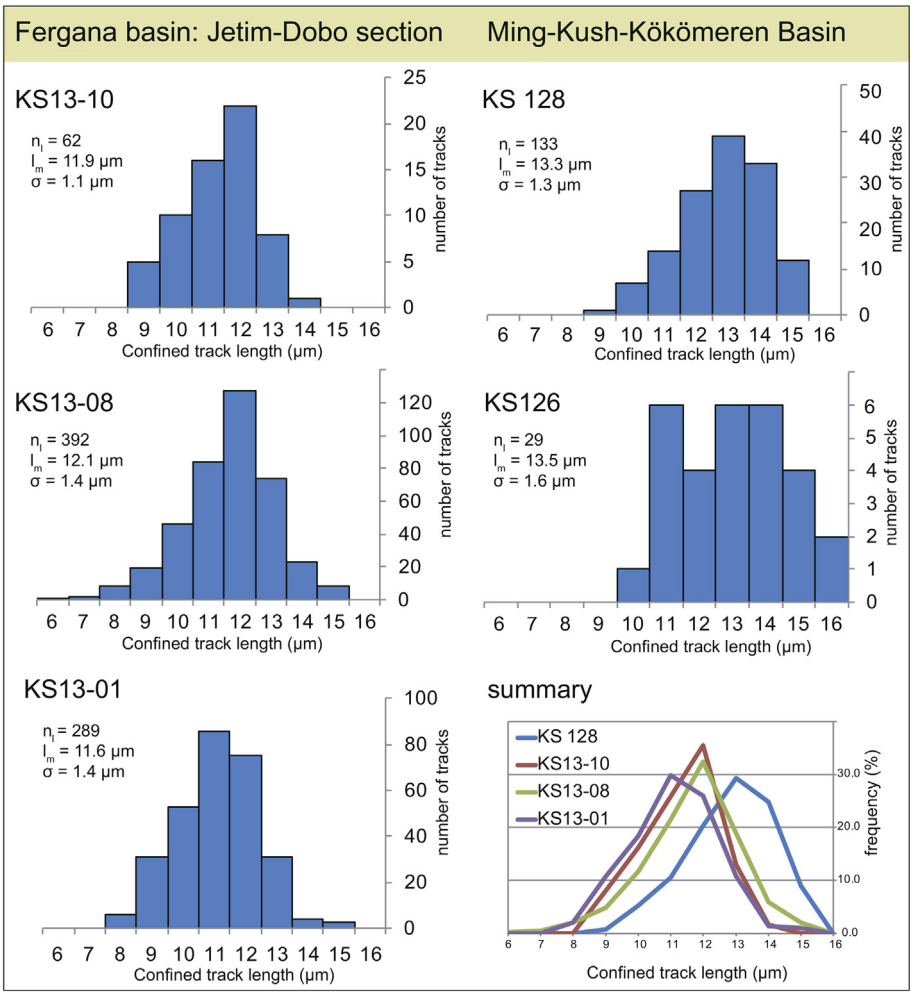

Figure 5. Track length histograms of detrital apatites in which it was possible to measure a sufficient number of confined track length data. The samples of two sedimentary sections are displayed. Jurassic samples KS-126 and KS-128 originate from the Ming-Kush section, while KS13-01 (Jurassic–Cretaceous transition), KS13-08 (Upper Cretaceous) and KS13-10 (Paleogene) are samples taken in the Fergana Basin (Jetim-Dobo section). A summary of the track length data of the samples with number of track lengths ($n > 50$) is displayed at the bottom right corner. This graph shows the track length data on a normalized vertical axis.

other detrital AFT studies in the south(western) Kyrgyz and Chinese Tien Shan (Wang et al., 2009; Glorie et al., 2011; Yang et al., 2014; Jia et al., 2015).

5.3. Tectonic evolution

5.3.1. Late Triassic–Middle Jurassic

Late Triassic–Early Jurassic basement cooling in the Tien Shan is recorded in multi-method low-temperature thermochronological studies of the Kyrgyz Tien Shan (e.g. De Grave et al., 2011a,b; Glorie and De Grave, 2016) and in the eastern Chinese Tien Shan (e.g. Jolivet et al., 2010; Zhang et al., 2016). Basement cooling is likely a result of the Late Triassic–Early Jurassic collision of the Qiangtang–Kunlun terranes with the Eurasian margin (Sengör, 1984; Watson et al., 1987; Yin and Harrison, 2000; Kapp et al., 2007). This phase of rapid basement cooling is detected by thermochronology studies on the mountain ranges adjacent to the Song-Kul plateau for example, in which AFT ages of ~231–193 Ma with high mean track lengths (~13 µm) and TFT ages of ~230–190 Ma are preserved (De Grave et al., 2011a), but are generally more scarce compared to the Cretaceous and Cenozoic AFT ages retrieved in the Kyrgyz Tien Shan, as visualized by Fig. 2 (Glorie and De Grave, 2016). Detrital AFT data indicate Late Triassic AFT age components in the southern Kyrgyz Tien Shan (~240–207 Ma) (Glorie et al., 2011; De Grave et al., 2012), southwestern Chinese Tien Shan (~219–205 Ma) (Sobel and Dumitru, 1997; Jia et al., 2015). Our study found that Late Triassic–Early Jurassic AFT ages are also preserved in the Jurassic sediments of the Ming-Kush-Kökömeren Basin, located in the NTS of Kyrgyzstan west of the Song-Kul plateau, and confirm this Late Triassic–Early Jurassic basement cooling phase.

The Late Triassic–Early Jurassic phase of rapid basement cooling coincides with the deposition of >3 km Jurassic sediments in the Yarkand-Fergana Basin (Sobel, 1999), maximum 680 m of Jurassic

Figure 4. Radial plots of AFT ages for the detrital samples from the Ming-Kush-Kökömeren, Fergana and Yarkand-Fergana basins, following the nomenclature of Allen et al. (2001) and Bachmanov et al. (2008). Central ages, minimum ages, dispersion and the P(χ^2) test were calculated with the RadialPlotter software (Vermeesch, 2009). '*n*' is the number of analysed apatite grains. The radial axis on the right of the plot reflects the corresponding single grain-ages in Ma and the left scale of the plot shows the standard deviations from the central age. The horizontal axis reflects a decreasing uncertainty on the single grain-ages from the left to the right. The light blue shaded segment corresponds to the depositional age of the sample, and the red line corresponds to the youngest U–Pb age component for the sample from the study of De Pelsmaeker et al. (2018). The available single grain confined track length data is displayed in yellow to red colours.

Please cite this article in press as: Nachtergaele, S., et al., Meso-Cenozoic tectonic evolution of the Talas-Fergana region of the Kyrgyz Tien Shan revealed by low-temperature basement and detrital thermochronology, Geoscience Frontiers (2017), https://doi.org/10.1016/j.gsf.2017.11.007

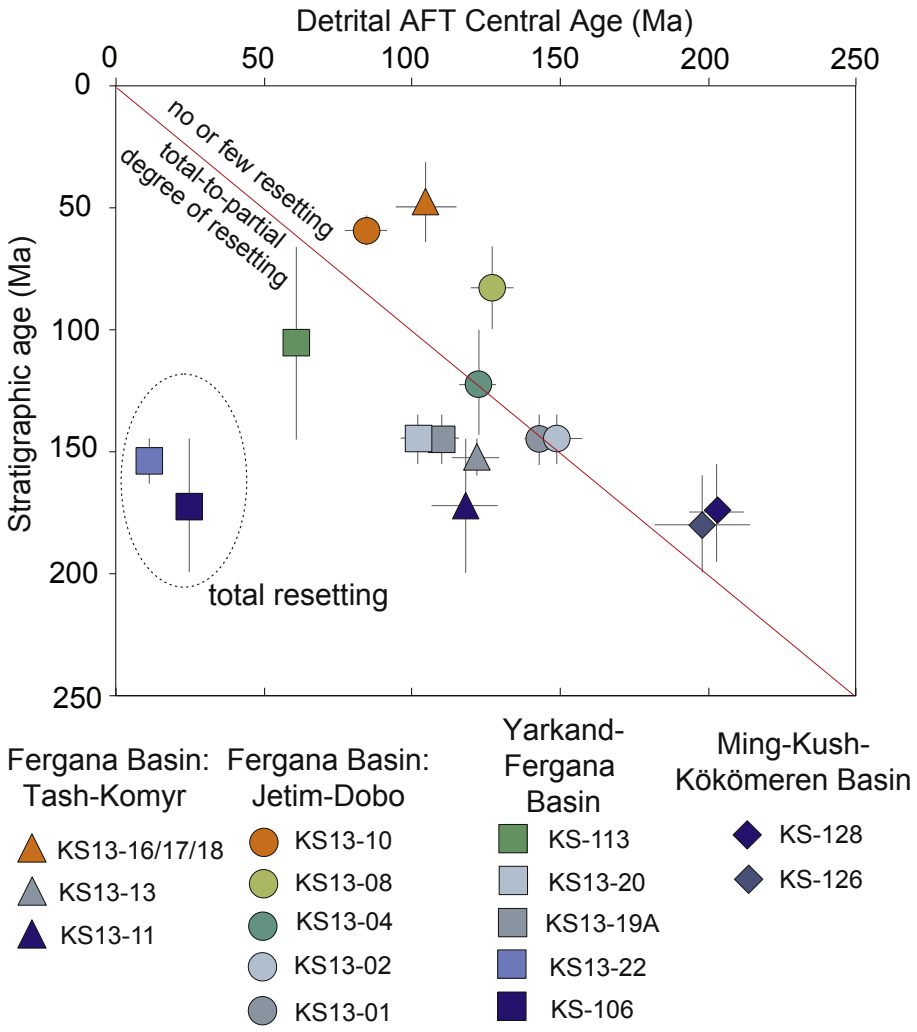

Figure 6. Plot of the detrital AFT results (with error bars) showing the relation between the central AFT age and stratigraphic age for each detrital sample. The red line indicates the 1:1 relationship between the vertical and horizontal axis. Extensive burial of the Jurassic samples of the Yarkand-Fergana Basin (e.g. KS-106 and KS13-22) below the AFT total annealing zone caused total resetting of the AFT age system. The Jurassic samples of the Ming-Kush-Kökömeren Basin plot on the right side of the red 1:1 line, indicating that the AFT age system of these samples are (almost) not reset due to post-depositional burial.

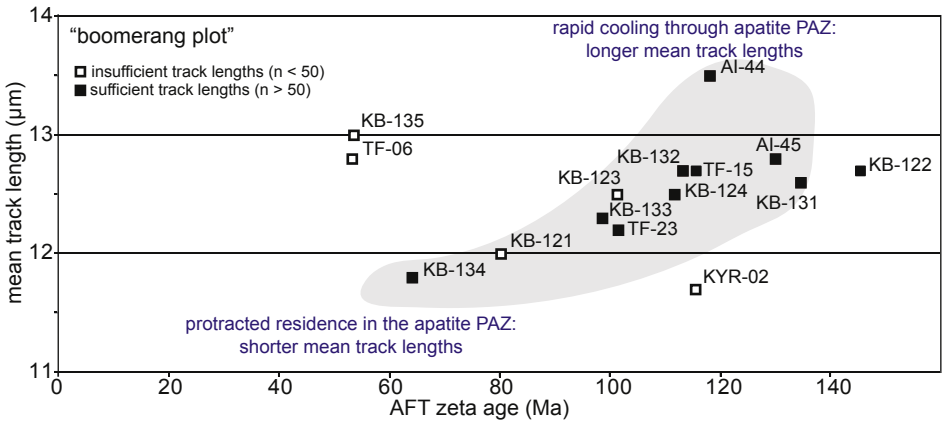

Figure 7. Boomerang plot (Green et al., 1986) on which the new basement AFT data of samples of the Northern Tien Shan and Middle Tien Shan are plotted. The mean track length and mean zeta age are displayed on the vertical and horizontal axis, respectively. Samples with sufficient track length data ($n > 50$) are displayed as full squares, while the samples with insufficient track length data ($n < 50$) are displayed as open squares. The boomerang plot expresses the relation between AFT age and mean track length, indicative for cooling rate through the apatite partial annealing zone. Rapid basement cooling (130–100 Ma) through the apatite partial annealing zone is characterized by higher mean track lengths. Lower track lengths are characteristic for samples with an AFT age between 100 and 65 Ma, which indicates that these samples experienced a protracted cooling through the apatite partial annealing zone.

Please cite this article in press as: Nachtergaele, S., et al., Meso-Cenozoic tectonic evolution of the Talas-Fergana region of the Kyrgyz Tien Shan revealed by low-temperature basement and detrital thermochronology, Geoscience Frontiers (2017), https://doi.org/10.1016/j.gsf.2017.11.007

sediments in the Ming-Kush-Kökömeren Basin, and the deposition of an alluvial fan conglomerate around 215 Ma in the Tarim (Dumitru et al., 2001) and Kuqa (Jolivet et al., 2013) basins. This phase of basement cooling is coeval as well with a stage of strike-slip movements along the TFF during the Early–Middle Jurassic with an estimated fault displacement up to 70 km (Alexeiev et al., 2017). Several Jurassic $^{40}Ar/^{39}Ar$ ages obtained on synkinematic mica of (mylonitic) granitoids, exposed in the TFF, provide evidence for fault activity at that time (Konopelko et al., 2013; Rolland et al., 2013). No new low-temperature thermochronological evidence for an Late Triassic–Early Jurassic deformation episode is found in the analysed basement samples along the TFF, suggesting that the basement samples experienced a younger thermal overprint and/or post Early Jurassic denudation.

5.3.2. Late Jurassic–Cretaceous

Based on our basement results and in comparison with earlier published AFT data of the Kyrgyz Tien Shan as discussed in Section 5.1, we propose that the Kyrgyz Tien Shan east of the TFF experienced rapid basement cooling with associated topography building and exhumation during the Late Jurassic–Early Cretaceous (>130–100 Ma), followed by slow basement cooling during the Late Cretaceous.

Additional arguments for an uplifted, reactivated Tien Shan east of the TFF can be found in (1) the distribution pattern of the sedimentary deposits in and adjacent to the Tien Shan and (2) provenance indicators in the Cretaceous and early Paleogene sediments of the Tien Shan as outlined below. In the NTS and MTS east of the TFF, Late Jurassic and Cretaceous sediments are generally absent and also in the Turpan, southern Junggar, and northern Tarim basins to the east, a hiatus in the sedimentary record occurred from 120 to 100 Ma (Hendrix et al., 1992). This is in contrast to the Fergana, Yarkand-Fergana and northwestern Tarim basins west of the TFF, where an almost continuous sedimentary record exist of Jurassic to Cenozoic sediments (Clarke, 1984; Lee, 1985; Sobel, 1999; De Pelsmaeker et al., 2018). A recent sediment provenance study by De Pelsmaeker et al. (2018) reports detrital zircon U–Pb ages of the same Meso-Cenozoic stratigraphic sections and samples as discussed in this study. Their study indicates a gradual shift in sediment provenance during the Cretaceous based on the increasing dominance of Late Ordovician–Silurian single grain U–Pb ages and decreasing dominance of Pennsylvanian–Permian single grain U–Pb ages in the sediments from the Fergana Basin from the Late Jurassic over the Cretaceous to the early Paleogene. Late Ordovician–Early Silurian zircon U–Pb ages are also reported in the Chinese part of the Yarkand-Fergana Basin by Yang et al. (2014). Because Late Ordovician–Silurian crystalline basement rocks are almost absent in the STS, but widespread in the NTS and in the MTS, it is thought that the NTS and MTS (mainly the Kyrgyz parts located east of the TFF) became the dominant sediment source for the Fergana basin during the Cretaceous (De Pelsmaeker et al., 2018). A setting of uplift and exhumation of the NTS and MTS – with a Cretaceous AFT cooling signature – is in agreement with the Cretaceous AFT central ages found in the limited to non-reset Late Cretaceous (KS13-08) and early Paleogene (KS13-10 and pooled KS13-16/17/18) samples of both sections from the Fergana Basin (see Section 5.2). The TFF may have therefore played a pivotal role in the tectonic evolution and sediment distribution pattern of the Tien Shan.

In general, the discussed Early Cretaceous rapid basement cooling (130–100 Ma) in the Tien Shan may be related to the closure of the Bangong Ocean between Lhasa and Qiangtang ('soft collision') around 140–130 Ma (Zhu et al., 2016) and eventual slab break off around ~113 ± 5 Ma (Hendrix et al., 1992; Kapp et al., 2007; Zhu et al., 2011, 2016; Chen et al., 2014; Glorie and De Grave, 2016). In addition, the Jurassic–Cretaceous geodynamic evolution of Central Asia was marked by the diachronous closure of the Mongol-Okhotsk Ocean, connecting Mongolia–North China to Siberia (Zorin, 1999; Daoudene et al., 2009; Metelkin et al., 2010, 2012; Wilhem et al., 2012). Y.T. Yang et al. (2015) found that the major part of the Mongol-Okhotsk Ocean closed on a relative short time scale (10 Ma) around the latest Jurassic–earliest Cretaceous transition, before complete closure in the Early Cretaceous contemporaneously with the collision of Lhasa to Eurasia. However, the implications of the closure of the Mongol-Okhotsk Ocean on exhumation events in Kyrgyzstan are still debated, but it is accepted that the closure of the Mongol-Okhotsk ocean and collapse of the Mongol Okhotsk orogeny mainly affected the areas to the northeast of the Tien Shan, such as the Altai-Sayan region (De Grave et al., 2007, 2009, 2013; Jolivet et al., 2013; Glorie and De Grave, 2016), Gobi Altai (Vassallo et al., 2007; Li et al., 2016) and eastern Mongolia (Daoudene et al., 2009). To summarize, it is most likely that the observed accelerated basement exhumation around 130–100 Ma (Fig. 7) is illustrative for the entire Central Asian geodynamic evolution, but it cannot be ruled out whether the Mongol-Okhotsk orogeny or Lhasa collision (or a combination of both) was the main cause of more rapid basement cooling in the Kyrgyz Tien Shan.

5.3.3. Cenozoic

The most recent reactivation of the Tien Shan initiates in the Oligocene–early Miocene, during which the India-Eurasia convergence caused major tectonic reactivation in large swathes of Central Asia (Molnar and Tapponier, 1975; Aitchison et al., 2007; De Grave et al., 2007; Bande et al., 2015b). During this late Cenozoic reactivation, the TFF accumulated approximately 60 km of slip (Burtman et al., 1996; Alexeiev et al., 2017), which was accommodated by the development of mountain building along the TFF and a clockwise rotation of the Fergana Basin (Thomas et al., 1993; Bande et al., 2015b). The late Cenozoic reactivation is supported by a large dataset of basement and detrital AFT studies in the Kyrgyz Tien Shan (Bullen et al., 2001; Sobel et al., 2006a,b; Glorie et al., 2010, 2011, 2012b; De Grave et al., 2011a, 2012, 2013; Macaulay et al., 2013, 2014; Bande et al., 2015b, 2017; De Pelsmaeker et al., 2015), northern Pamir front (Käßner et al., 2016), central Chinese Tien Shan (Dumitru et al., 2001; Wang et al., 2009; Jolivet et al., 2010), and the SW Chinese Tien Shan (Sobel et al., 2006a; Yang et al., 2014; Jia et al., 2015) and by various structural studies (e.g. Coutand et al., 2002). Intensification of basement exhumation initiated since the late Miocene (Sobel et al., 2006a; Glorie et al., 2010, 2011; Macaulay et al., 2014; Glorie and De Grave, 2016). Two partially-to-totally reset Jurassic detrital samples (KS13-22 and KS-106) of the Yarkand-Fergana Basin exhibit Oligocene (~25 Ma) and Miocene (~11 Ma) AFT central ages and constrain the timing of basin inversion. These results are consistent with the low-temperature thermochronological data from Bande et al. (2017) in which they found an Oligocene (~25 Ma) onset and late Miocene intensification of Cenozoic deformation of the western Kyrgyz Tien Shan.

6. Conclusion

This study presents apatite fission track (AFT) results for 20 crystalline basement rocks samples, 13 Mesozoic and 4 Early Cenozoic detrital sediments. Additional zircon (U–Th)/He and apatite U–Pb analyses were carried out on 2 crystalline basement rocks (AI-45 and KYR-05) as well. This multi-method approach allows to put further constraints on the Mesozoic evolution of the Kyrgyz Tien Shan. The following conclusions could be drawn:

Please cite this article in press as: Nachtergaele, S., et al., Meso-Cenozoic tectonic evolution of the Talas-Fergana region of the Kyrgyz Tien Shan revealed by low-temperature basement and detrital thermochronology, Geoscience Frontiers (2017), https://doi.org/10.1016/j.gsf.2017.11.007

(1) Evidence of a Triassic–Early Jurassic basement exhumation event is preserved in Jurassic sediments exposed in the Ming-Kush-Kökömeren Basin. These sediments experienced insufficient post-depositional heating in order to reset the inherited AFT age components. High mean track lengths (~13.5 μm) characterize several Jurassic samples in the basin with central AFT ages ~200 Ma. Rapid basement cooling around the Triassic–Jurassic boundary might be linked to the closure of the Paleo-Tethys Ocean, more specifically, to far-field effects of the collision of the Tibetan Qiangtang Block to the Eurasian margin.
(2) Apatite fission track data, zircon (U–Th)/He ages and associated thermal history models obtained on granitoid basement samples exposed in the Middle and Northern Tien Shan east of the Talas-Fergana Fault indicate increased basement cooling rates during the Early Cretaceous (Barremian-Albian, ~130–100 Ma). This is possibly an effect of the Lhasa collision to the Eurasian margin.
(3) In the same region, apatite fission track length data (~12 μm) are particularly low for basement rocks with Late Cretaceous AFT ages, indicating slow cooling through the apatite partial annealing zone. These slowly cooled basement rocks of the Northern and Middle Tien Shan east of the TFF could represent the sediment source for the Late Cretaceous–Paleogene sediments deposited in the Fergana Basin based on their inherited Cretaceous AFT single grain ages.
(4) The majority of the Mesozoic sediments of the Fergana Basin and especially the Yarkand-Fergana Basin experienced post-depositional burial reheating. This reheating caused fission track annealing, as evidenced by a decreasing central age and mean track length of the (Mesozoic) samples down in the stratigraphic section. In some cases, the samples even experienced reheating back in the apatite total annealing zone, effectively resetting the AFT system. For example, Jurassic sediments of the Yarkand-Fergana Basin yield reset AFT ages of 25.1 ± 1.8 Ma and 11.4 ± 0.9 Ma and constrain the timing of basin inversion in the Yarkand-Fergana Basin and late Cenozoic deformation in the western Kyrgyz Tien Shan as caused by the India-Eurasia collision.

Acknowledgements

This research was supported by a Ghent University project (BOF 015B1309) and by the DARIUS program. SG's contribution was supported by ARC DP150101730 and forms TRAX record 387. F.I. Zhimulev's contribution was supported by state assignment project No. 0330-2016-0015. We are indebted to Dr. Guido Vittiglio and Bart Van Houdt for their help with irradiations and neutron dosimetry at the Belgian Nuclear Research Centre in Mol (SCK-CEN, BR1 facility) and to Dr. Vladislav Batalev, Prof. Dr. Cécile Robin, A. Dransart Laborde, C. Ormukov, Dr. E. Bataleva and Sasha Ryabinin for their help during the field expeditions. We are also very grateful to Ann-Eline Debeer for her assistance in our laboratory in Ghent. Gerben Van Ranst is thanked for the development of the new Nikon fission track microscope system and his help with Adobe Illustrator. We would like to thank Dr. Christopher Spencer for editorial handling and anonymous reviewers for constructive comments. This paper is dedicated to our friend and colleague Vlad Batalev who very recently deceased at a far too young age.

Appendix A. Supplementary data

Supplementary data related to this article can be found at https://doi.org/10.1016/j.gsf.2017.11.007.

References

Aitchison, J.C., Ali, J.R., Davis, A.M., 2007. When and where did India and Asia collide? Journal of Geophysical Research 112, 1–19. https://doi.org/10.1029/2006JB004706.

Alekseev, D.V., Degtyarev, K.E., Kotov, A.B., Sal'nikova, E.B., Tretyakov, A.A., Yakovleva, S.Z., Anisimova, I.V., Shatagin, K.N., 2009. Late Paleozoic subductional and collisional igneous complexes in the Naryn segment of the Middle Tien Shan (Kyrgyzstan). Doklady Earth Sciences 427, 760–763. https://doi.org/10.1134/S1028334X09050122.

Alexeiev, D.V., Bykadorov, V.A., Volozh, Y.A., Sapozhnikov, R.B., 2017. Kinematic analysis of Jurassic Grabens of Southern Turgai and the role of the Mesozoic Stage in the evolution of the Karatau – Talas – Ferghana Strike-Slip Fault, Southern Kazakhstan and Tian Shan. Geotectonics 51, 105–120. https://doi.org/10.1134/S0016852117020029.

Alexeiev, D.V., Kröner, A., Hegner, E., Rojas-agramonte, Y., Biske, Y.S., Wong, J., Geng, H.Y., Ivleva, E.A., Mühlberg, M., Mikolaichuk, A.V., Liu, D., 2016. Middle to Late Ordovician arc system in the Kyrgyz Middle Tianshan: from arc-continent collision to subsequent evolution of a Palaeozoic continental margin. Gondwana Research 39, 261–291. https://doi.org/10.1016/j.gr.2016.02.003.

Allen, M.B., Alsop, G.I., Zhemchuzhnikov, V.G., 2001. Dome and basin refolding and transpressive inversion along the Karatau Fault System, southern Kazakstan. Journal of the Geological Society, London 158, 83–95.

Angiolini, L., Zanchi, A., Zanchetta, S., Nicora, A., Vezzoli, G., 2013. The Cimmerian geopuzzle: new data from South Pamir. Terra Nova 25, 352–360. https://doi.org/10.1111/ter.12042.

Bachmanov, D.M., Trifonov, V.G., Mikolaichuk, A.V., Vishnyakov, F.A., Zarshchikov, A.A., 2008. The Ming-Kush-Kokomeren zone of recent transpression in the Middle Tien Shan. Geotectonics 42, 186–205. https://doi.org/10.1134/S0016852108030035.

Bande, A., Radjabov, S., Sobel, E.R., Sim, T., 2015a. Cenozoic palaeoenvironmental and tectonic controls on the evolution of the northern Fergana Basin. Geological Society London Special Publications 427.

Bande, A., Sobel, E.R., Mikolaichuk, A., Schmidt, A., Stockli, D.F., 2017. Exhumation history of the western Kyrgyz Tien Shan: implications for intramontane basin formation. Tectonics 36, 1–18. https://doi.org/10.1002/2016TC004284.

Bande, A., Sobel, E.R., Mikolaichuk, A., Torres Acosta, V., 2015b. Talas – Fergana Fault Cenozoic timing of deformation and its relation to Pamir indentation. Geological Society London Special Publications 427.

Barbarand, J., Carter, A., Wood, I., Hurford, T., 2003. Compositional and structural control of fission-track annealing in apatite. Chemical Geology 198, 107–137. https://doi.org/10.1016/S0009-2541(02)00424-2.

Bazhenov, M.L., Burtman, V.S., Dvorova, A.V., 1999. Permian paleomagnetism of the Tien Shan fold belt, Central Asia: post-collisional rotations and deformation. Tectonophysics 312, 303–329. https://doi.org/10.1016/S0040-1951(99)00181-X.

Belgovskiy, G.L., Ektova, L.A., Maslova, E.V., 1958. Explanation Note to the Sheet K-43-XXXIII of the Geological Map of USSR, Scale 1:200 000, 10 pp (in Russian).

Biske, Y.S., Konopelko, D.L., Seltmann, R., 2013. Geodynamics of Late Paleozoic magmatism in the Tien Shan and its framework. Geotectonics 47, 291–309. https://doi.org/10.1134/S001685211304002X.

Biske, Y.S., Seltmann, R., 2010. Paleozoic Tian-Shan as a transitional region between the Rheic and Urals-Turkestan oceans. Gondwana Research 17, 602–613. https://doi.org/10.1016/j.gr.2009.11.014.

Bosboom, R., Dupont-Nivet, G., Aminov, J., 2015. Late Eocene paleogeography of the Proto-Paratethys Sea in Central Asia (NW China, S Kyrgyzstan and SW Tajikistan). Darius. https://doi.org/10.1144/SP427.11.

Bullen, M.E., Burbank, D.W., Garver, J.I., Abdrakhmatov, K.Y., 2001. Late Cenozoic tectonic evolution of the northwestern Tien Shan: new age estimates for the initiation of mountain building. Geological Society of America Bulletin 113, 1544–1559. https://doi.org/10.1130/0016-7606(2001)113<1544:LCTEOT>2.0.CO;2.

Burtman, V.S., 2015. Tectonics and geodynamics of the Tian Shan in the Middle and Late Paleozoic. Geotectonics 49, 302–319. https://doi.org/10.1134/S0016852115040020.

Burtman, V.S., 2010. Tien Shan, Pamir, and Tibet: history and geodynamics of phanerozoic oceanic basins. Geotectonics 44, 388–404. https://doi.org/10.1134/S001685211005002X.

Burtman, V.S., 1980. Faults of Middle Asia. American Journal of Science 280, 725–744.

Burtman, V.S., Skobelev, S.F., Molnar, P., 1996. Late Cenozoic slip on the Talas-Ferghana fault, the Tien Shan, central Asia. Geological Society of America Bulletin 108, 1004–1021.

Carlson, W.D., Donelick, R.A., Ketcham, R.A., 1999. Variability of apatite fission-track anneling kinetics; I, Experimental results. American Mineralogist 84, 1213–1223.

Carroll, A.R., Graham, S.A., Hendrix, M.S., Ying, D., Zhou, D., 1995. Late Paleozoic tectonic amalgamation of northwestern China: sedimentary record of the northern Tarim, northwestern Turpan, and southern Junggar Basins. Geological Society of America Bulletin 107, 571–594. https://doi.org/10.1130/0016-7606(1995)107<0571:LPTAON>2.3.CO;2.

Chen, Y., Zhu, D., Zhao, Z., Meng, F., Wang, Q., Santosh, M., Wang, L., Dong, G., Mo, X., 2014. Slab breakoff triggered ca. 113 Ma magmatism around Xainza area of the Lhasa Terrane, Tibet. Gondwana Research 26, 449–463. https://doi.org/10.1016/j.gr.2013.06.005.

Chew, D.M., Petrus, J.A., Kamber, B.S., 2014. U-Pb LA-ICPMS dating using accessory mineral standards with variable common Pb. Chemical Geology 363, 185–199. https://doi.org/10.1016/j.chemgeo.2013.11.006.

Chew, D.M., Spikings, R.A., 2015. Geochronology and thermochronology using apatite: time and temperature, lower crust to surface. Elements 11, 189–194. https://doi.org/10.2113/gselements.11.3.189.

Chew, D.M., Sylvester, P.J., Tubrett, M.N., 2011. U-Pb and Th-Pb dating of apatite by LA-ICPMS. Chemical Geology 280, 200–216. https://doi.org/10.1016/j.chemgeo.2010.11.010.

Clarke, J.W., 1984. Geology and Possible Uranium Deposits of the Fergana Region of Soviet Central Asia. United States Dep. Inter. Geol. Surv., pp. 84–513

Coutand, I., Strecker, M.R., Arrowsmith, J.R., Hilley, G., Thiede, R.C., Korjenkov, A., Omuraliev, M., 2002. Late Cenozoic tectonic development of the intramontane Alai Valley, (Pamir-Tien Shan region, central Asia): an example of intracontinental deformation due to the Indo-Eurasia collision. Tectonics 21. https://doi.org/10.1029/2002TC001358.

Daoudene, Y., Gapais, D., Ledru, P., Cocherie, A., Hocquet, S., Donskaya, T.V., 2009. The Ereendavaa Range (north-eastern Mongolia): an additional argument for Mesozoic extension throughout eastern Asia. International Journal of Earth Sciences 98, 1381–1393. https://doi.org/10.1007/s00531-008-0412-2.

De Corte, F., Bellemans, F., Van den haute, P., Ingelbrecht, C., Nicholl, C., 1998. A New U Doped Glass Certified by the European Commission for the Calibration of Fission Track Dating. Kluwer Academic Publishers, pp. 67–78.

De Grave, J., Buslov, M.M., Van Den Haute, P., Metcalf, J., Mcwilliams, M.O., Grave, J.D.E., Buslov, M.M., Van den haute, P., 2009. Multi-method chronometry of the Teletskoye graben and its basement, Siberian Altai Mountains: new insights on its thermo-tectonic evolution email alerting service permission subscribe click here to subs. Geological Society London Special Publications 324, 237–259. https://doi.org/10.1144/SP324.17.

De Grave, J., Buslov, M.M., Van den haute, P., 2007. Distant effects of India-Eurasia convergence and Mesozoic intracontinental deformation in Central Asia: constraints from apatite fission-track thermochronology. Journal of Asian Earth Sciences 29, 188–204. https://doi.org/10.1016/j.jseaes.2006.03.001.

De Grave, J., Glorie, S., Buslov, M.M., Izmer, A., Fournier-Carrie, A., Batalev, V.Y., Vanhaecke, F., Elburg, M., Van den haute, P., 2011a. The thermo-tectonic history of the Song-Kul plateau, Kyrgyz Tien Shan: constraints by apatite and titanite thermochronometry and zircon U/Pb dating. Gondwana Research 20, 745–763. https://doi.org/10.1016/j.gr.2011.03.011.

De Grave, J., Glorie, S., Buslov, M.M., Stockli, D.F., McWilliams, M.O., Batalev, V.Y., Van den haute, P., 2013. Thermo-tectonic history of the Issyk-Kul basement (Kyrgyz Northern Tien Shan, Central Asia). Gondwana Research 23, 998–1020. https://doi.org/10.1016/j.gr.2012.06.014.

De Grave, J., Glorie, S., Ryabinin, A., Zhimulev, F., Buslov, M.M., Izmer, A., Elburg, M., Vanhaecke, F., Van den haute, P., 2012. Late Palaeozoic and Meso-Cenozoic tectonic evolution of the southern Kyrgyz Tien Shan: constraints from multi-method thermochronology in the Trans-Alai, Turkestan-Alai segment and the southeastern Ferghana Basin. Journal of Asian Earth Sciences 44, 149–168. https://doi.org/10.1016/j.jseaes.2011.04.019.

De Grave, J., Glorie, S., Zhimulev, F.I., Buslov, M.M., Elburg, M., Vanhaecke, F., Van Den, P., 2011b. Emplacement and exhumation of the Kuznetsk-Alatau basement (Siberia): implications for the tectonic evolution of the Central Asian Orogenic Belt and sediment supply to the Kuznetsk, Minusa and West Siberian Basins. Terra Nova 23, 248–256. https://doi.org/10.1111/j.1365-3121.2011.01006.x.

De Grave, J., Van den haute, P., 2002. Denudation and cooling of the Lake Teletskoye Region in the Altai Mountains (South Siberia) as revealed by apatite fission-track thermochronology. Tectonophysics 349, 145–159.

De Pelsmaeker, E., 2018. Source-to-sink interpretations of the Jurassic to Paleogene sedimentary record (or sediments) of the Kyrgyz Tien Shan: insights from sedimentological and detrital zircon U-Pb analyses. Gondwana Research 54, 180–204.

De Pelsmaeker, E., Glorie, S., Buslov, M.M., Zhimulev, F.I., Poujol, M., Korobkin, V.V., Vanhaecke, F., Vetrov, E.V., De Grave, J., 2015. Late-Paleozoic emplacement and Meso-Cenozoic reactivation of the southern Kazakhstan granitoid basement. Tectonophysics 662, 416–433. https://doi.org/10.1016/j.tecto.2015.06.014.

Dumitru, T.A., Zhou, D., Chang, E.Z., Graham, S.A., Hendrix, M.S., Sobel, E.R., Carroll, A.R., 2001. Uplift, exhumation, and deformation in the Chinese Tian Shan. Memoirs – Geological Society of America 194, 71–99. https://doi.org/10.1130/0-8137-1194-0.71.

Evans, N.J., Byrne, J.P., Keegan, J.T., Dotter, L.E., 2005. Determination of uranium and thorium in zircon, apatite, and fluorite: application to laser (U–Th)/He thermochronology. Journal of Analytical Chemistry 60, 1300–1307.

Farley, K.A., 2002. (U-Th)/He dating: techniques, calibrations, and applications. Reviews in Mineralogy and Geochemistry 18. https://doi.org/10.2138/rmg.2002.47.18.

Farley, K.A., Wolf, R.A., Silver, L.T., 1996. The effects of long alpha-stopping distances on (U-Th)/He ages. Geochimica et Cosmochimica Acta 60, 4223–4229.

Filippova, I.B., Bush, V.A., Didenko, A.N., 2002. Middle Paleozoic subduction belts: the leading factor in the formation of the Central Asian fold-and-thrust belt. Russian Journal of Earth Sciences 3, 405–426.

Galbraith, R.F., 1981. On statistical models for fission track counts. Mathematical Geology 13, 471–478.

Galbraith, R.F., Green, P.F., 1990. Estimating the component ages in a finite mixture. International Journal of Radiation Applications and Instrumentation. Part D 17, 197–206. https://doi.org/10.1016/1359-0189(90)90035-V.

Galbraith, R.F., Laslett, G.M., 1993. Statistical models for mixed fission track ages. International Journal of Radiation Applications and Instrumentation. Part D 21, 459–470. https://doi.org/10.1016/1359-0189(93)90185-C.

Gallagher, K., 2012. Transdimensional inverse thermal history modeling for quantitative thermochronology. Journal of Geophysical Research – Solid Earth 117, 1–16. https://doi.org/10.1029/2011JB008825.

Gillespie, J., Glorie, S., Xiao, W., Zhang, Z., Collins, A.S., Evans, N., Mcinnes, B., De Grave, J., 2017. Mesozoic reactivation of the Beishan, southern Central Asian Orogenic Belt: insights from low-temperature thermochronology. Gondwana Research 43, 107–122. https://doi.org/10.1016/j.gr.2015.10.004.

Gleadow, A., Harrison, M., Kohn, B., Lugo-Zazueta, R., Phillips, D., 2015. The Fish Canyon Tuff: a new look at an old low-temperature thermochronology standard. Earth and Planetary Science Letters 424, 95–108. https://doi.org/10.1016/j.epsl.2015.05.003.

Gleadow, A.J.W., Duddy, I.R., Green, P.F., Lovering, J.F., 1986. Confined fission track lengths in apatite: a diagnostic tool for thermal history analysis. Contributions to Mineralogy and Petrology 94, 405–415. https://doi.org/10.1007/BF00376334.

Glorie, S., Alexandrov, I., Nixon, A., Jepson, G., Gillespie, J., Jahn, B.-M., 2017. Thermal and exhumation history of Sakhalin Island (Russia) constrained by apatite U-Pb and fission track thermochronology. Journal of Asian Earth Sciences 143, 326–342. https://doi.org/10.1016/j.jseaes.2017.05.011.

Glorie, S., De Grave, J., 2016. Exhuming the Meso-Cenozoic Kyrgyz Tianshan and Siberian Altai-Sayan: a review based on low-temperature thermochronology. Geoscience Frontiers 7, 155–170. https://doi.org/10.1016/j.gsf.2015.04.003.

Glorie, S., De Grave, J., Buslov, M.M., Elburg, M.A., Stockli, D.F., Gerdes, A., Van Den Haute, P., 2010. Multi-method chronometric constraints on the evolution of the Northern Kyrgyz Tien Shan granitoids (Central Asian Orogenic Belt): from emplacement to exhumation. Journal of Asian Earth Sciences 38, 131–146. https://doi.org/10.1016/j.jseaes.2009.12.009.

Glorie, S., De Grave, J., Buslov, M.M., Zhimulev, F.I., Elburg, M.A., Van den haute, P., 2012a. Structural control on Meso-Cenozoic tectonic reactivation and denudation in the Siberian Altai: insights from multi-method thermochronometry. Tectonophysics 544–545, 75–92. https://doi.org/10.1016/j.tecto.2012.03.035.

Glorie, S., De Grave, J., Buslov, M.M., Zhimulev, F.I., Stockli, D.F., Batalev, V.Y., Izmer, A., Van Den Haute, P., Vanhaecke, F., Elburg, M.A., 2011. Tectonic history of the Kyrgyz South Tien Shan (Atbashi-Inylchek) suture zone: the role of inherited structures during deformation-propagation. Tectonics 30. https://doi.org/10.1029/2011TC002949.

Glorie, S., De Grave, J., Delvaux, D., Buslov, M.M., Zhimulev, F.I., Vanhaecke, F., Elburg, M.A., 2012b. Tectonic history of the Irtysh shear zone (NE Kazakhstan): new constraints from zircon U/Pb dating, apatite fission track dating and palaeostress analysis. Journal of Asian Earth Sciences 45, 138–149. https://doi.org/10.1016/j.jseaes.2011.09.024.

Green, P.F., 1981. A new look at statistics in fission-track dating. Nuclear Tracks 5, 77–86.

Green, P.F., Duddy, I.R., Gleadow, A.I.W., Lovering, J.F., 1989. Apatite Fission-track Analysis as a Paleotemperature Indicator for Hydrocarbon Exploration. In: Thermal History of Sedimentary Basins, pp. 181–195.

Green, P.F., Duddyi, I.R., Gleadow, A.J.W., Tingate, P.R., Laslett, G.M., 1986. Thermal annealing of fission tracks in apatite 1. A qualitative description. Chemical Geology 59, 237–253.

Guenther, W., Reiners, P.W., Ketcham, R.A., Nasdala, L., Giester, G., 2013. Helium diffusion in natural zircon: radiation damage anisotropy, and the interpretation of zircon (U-Th)/He thermochronology. American Journal of Science 313, 145–198. https://doi.org/10.2475/03.2013.01.

Harrison, T.M., Duncan, I.A.N., Mcdougall, I.A.N., 1985. Diffusion of ^{40}Ar in biotite: temperature, pressure and compositional effects. Geochimica et Cosmochimica Acta 49, 2461–2468.

Hasebe, N., Barbarand, J., Jarvis, K., Carter, A., Hurford, A.J., 2004. Apatite fission-track chronometry using laser ablation ICP-MS. Chemical Geology 207, 135–145. https://doi.org/10.1016/j.chemgeo.2004.01.007.

Hendrix, M.S., 2000. Evolution of Mesozoic sandstone compositions, southern Junggar, northern Tarim and western Turpan basins, northwest China: a detrital record of the ancestral Tian Shan. Journal of Sedimentary Research 70, 520–532.

Hendrix, M.S., Graham, S.A., Carroll, A.R., Sobel, E.R., McKnight, C.L., Schulein, B.J., Wang, Z., 1992. Sedimentary record and climatic implications of recurrent deformation in the Tian Shan: evidence from Mesozoic strata of the north Tarim, south Junggar, and Turpan basins, northwest China. Geological Society of America Bulletin 104, 53–79. https://doi.org/10.1130/0016-7606(1992)104<0053:SRACIO>2.3.CO;2.

Hurford, A.J., 1990. Standardization of fission track dating calibration: recommendation by the Fission Track Working Group of the I. U. G. S. Subcommission on geochronology. Chemical Geology 80, 171–178.

Hurford, A.J., Green, P.F., 1983. The zeta age calibration of fission-track dating. Chemical Geology 41, 285–317. https://doi.org/10.1016/S0009-2541(83)80026-6.

Hurford, A.J., Hammerschmidt, K., 1985. ^{40}Ar/^{39}Ar and K/Ar dating of the Bishop and Fish Canyon Tuffs: calibration ages for fission-track dating standards. Chemical Geology 58, 23–32. https://doi.org/10.1016/0168-9622(85)90024-7.

Jia, Y., Fu, B., Jolivet, M., Zheng, S., 2015. Cenozoic tectono-geomorphological growth of the SW Chinese Tian Shan: insight from AFT and detrital zircon U–Pb data. Journal of Asian Earth Sciences 111, 395–413. https://doi.org/10.1016/j.jseaes.2015.06.023.

Please cite this article in press as: Nachtergaele, S., et al., Meso-Cenozoic tectonic evolution of the Talas-Fergana region of the Kyrgyz Tien Shan revealed by low-temperature basement and detrital thermochronology, Geoscience Frontiers (2017), https://doi.org/10.1016/j.gsf.2017.11.007

Jolivet, M., 2015. Mesozoic tectonic and topographic evolution of Central Asia and Tibet: a preliminary synthesis. Geological Society London Special Publications 427.

Jolivet, M., Bourquin, S., Heilbronn, G., Robin, C., Barrier, L., Dabard, M., Jia, Y., De Pelsmaeker, E., Fu, B., 2015. The Upper Jurassic – Lower Cretaceous alluvial-fan deposits of the Kalaza Formation (Central Asia): tectonic pulse or increased aridity? Geological Society London Special Publications 427.

Jolivet, M., Dominguez, S., Charreau, J., Chen, Y., Li, Y., Wang, Q., 2010. Mesozoic and Cenozoic tectonic history of the central Chinese Tian Shan: reactivated tectonic structures and active deformation. Tectonics 29, 1–30. https://doi.org/10.1029/2010TC002712.

Jolivet, M., Heilbronn, G., Robin, C., Barrier, L., Bourquin, S., Guo, Z., Jia, Y., Guerit, L., Yang, W., Fu, B., 2013. Reconstructing the Late Palaeozoic – Mesozoic topographic evolution of the Chinese Tian Shan: available data and remaining uncertainties. Advances in Geosciences 37, 7–18. https://doi.org/10.5194/adgeo-37-7-2013.

Kapp, P., Decelles, P.G., Gehrels, G.E., Heizler, M., Ding, L., 2007. Geological records of the Lhasa-Qiangtang and Indo-Asian collisions in the Nima area of central Tibet. Geological Society of America Bulletin 119, 917–932. https://doi.org/10.1130/B26033.1.

Käßner, A., Ratschbacher, L., Jonckheere, R., Enkelmann, E., Khan, J., Sonntag, B., Gloaguen, R., Gadoev, M., Oimahmadov, I., 2016. Cenozoic intracontinental deformation and exhumation at the northwestern tip of the India-Asia collision—southwestern Tian Shan, Tajikistan, and Kyrgyzstan. Tectonics 35, 2171–2194. https://doi.org/10.1002/2015TC003897.Received.

Käßner, A., Ratschbacher, L., Pfänder, J.A., Hacker, B.R., Zack, G., Sonntag, B.L., Khan, J., Stanek, K.P., Gadoev, M., Oimahmadov, I., 2017. Proterozoic-Mesozoic history of the central Asian orogenic belt in the tajik and southwestern kyrgyz tian shan: U-Pb, 40Ar/39Ar, and fission-track geochronology and geochemistry of granitoids. Bulletin of the Geological Society of America 129, 281–303. https://doi.org/10.1130/B31466.1.

Ketcham, R.A., Carter, A., Donelick, R.A., Barbarand, J., Hurford, A.J., 2007. Improved modeling of fission-track annealing in apatite. American Mineralogist 92, 799–810. https://doi.org/10.2138/am.2007.2281.

Ketcham, R.A., Donelick, R.A., Carlson, W.D., 1999. Cariability of apatite fission-track anneling kinetics: III. Extrapolation to geological time scales. American Mineralogist 84, 1235–1255.

Khain, E.V., Bibikova, E.V., Salnikova, E.B., Kröner, A., Gibsher, A.S., Didenko, A.N., Degtyarev, K.E., Fedotova, A.A., 2003. The Palaeo-Asian ocean in the Neoproterozoic and early Palaeozoic: new geochronologic data and palaeotectonic reconstructions. Precambrian Research 122, 329–358.

Konopelko, D., Biske, G., Seltmann, R., Eklund, O., Belyatsky, B., 2007. Hercynian post-collisional A-type granites of the Kokshaal Range, Southern Tien Shan, Kyrgyzstan. Lithos 97, 140–160. https://doi.org/10.1016/j.lithos.2006.12.005.

Konopelko, D., Biske, G., Seltmann, R., Kiseleva, M., Matukov, D., Sergeev, S., 2008. Deciphering Caledonian events: timing and geochemistry of the Caledonian magmatic arc in the Kyrgyz Tien Shan. Journal of Asian Earth Sciences 32, 131–141. https://doi.org/10.1016/j.jseaes.2007.10.017.

Konopelko, D., Seltmann, R., Apayarov, F., Belousova, E., Izokh, A., Lepekhina, E., 2013. U – Pb – Hf zircon study of two mylonitic granite complexes in the Talas-Fergana fault zone, Kyrgyzstan, and Ar – Ar age of deformations along the fault. Journal of Asian Earth Sciences 73, 334–346. https://doi.org/10.1016/j.jseaes.2013.04.046.

Korzhenkov, A.M., Rogozhin, E.A., Xuhui, S., Qinjian, T., Yueren, X., 2014. Strong paleoearthquakes along the Talas-Fergana Fault, Kyrgyzstan. Geodesy and Geodynamics 5, 11–19. https://doi.org/10.3724/SP.J.1246.2014.01011.

Kröner, A., Alexeiev, D.V., Kovach, V.P., Rojas-agramonte, Y., Tretyakov, A.A., Mikolaichuk, A.V., 2017. Zircon ages, geochemistry and Nd isotopic systematics for the Palaeoproterozoic 2.3 – 1.8 Ga Kuilyu Complex, East Kyrgyzstan – the oldest continental basement fragment in the Tianshan orogenic belt. Journal of Asian Earth Sciences 135, 122–135. https://doi.org/10.1016/j.jseaes.2016.12.022.

Kröner, A., Alexeiev, D.V., Rojas-Agramonte, Y., Hegner, E., Wong, J., Xia, X., Belousova, E., Mikolaichuk, A.V., Seltmann, R., Liu, D., Kiselev, V.V., 2013. Mesoproterozoic (Grenville-age) terranes in the Kyrgyz North Tianshan: zircon ages and Nd-Hf isotopic constraints on the origin and evolution of basement blocks in the southern Central Asian Orogen. Gondwana Research 23, 272–295. https://doi.org/10.1016/j.gr.2012.05.004.

Lee, K.Y., 1985. Geology of the Tarim Basin with Special Emphasis on Petroleum Deposits. U.S. Geol. Surv. Reson. Virginia. Open-File Rep., pp. 85–616.

Li, K., Jolivet, M., Zhang, Z., Li, J., Tang, W., 2016. Long-term exhumation history of the Inner Mongolian Plateau constrained by apatite fission track analysis. Tectonophysics 666, 121–133. https://doi.org/10.1016/j.tecto.2015.10.020.

Liu, D., Guo, Z., Jolivet, M., Cheng, F., Song, Y., Zhang, Z., 2014. Petrology and geochemistry of Early Permian volcanic rocks in South Tian Shan, NW China: implications for the tectonic evolution and Phanerozoic continental growth. International Journal of Earth Sciences. https://doi.org/10.1007/s00531-013-0994-1.

Loury, C., Rolland, Y., Cenki-Tok, B., Lanari, P., Guillot, S., 2016. Late Paleozoic evolution of the South Tien Shan: insights from P-T estimates and allanite geochronology on retrogressed eclogites (Chatkal range, Kyrgyzstan). Journal of Geodynamics 96, 62–80. https://doi.org/10.1016/j.jog.2015.06.005.

Macaulay, E.A., Sobel, E.R., Mikolaichuk, A., Kohn, B., Stuart, F.M., 2014. Cenozoic deformation and exhumation history of the Central Kyrgyz Tien Shan. Tectonics 33, 135–165. https://doi.org/10.1002/2013TC003376.

Macaulay, E.A., Sobel, E.R., Mikolaichuk, A., Landgraf, A., Kohn, B., Stuart, F., 2013. Thermochronologic insight into late Cenozoic deformation in the basement-cored Terskey Range, Kyrgyz Tien Shan. Tectonics 32, 487–500. https://doi.org/10.1002/tect.20040.

McDowell, F.W., McIntosh, W.C., Farley, K.A., 2005. A precise ^{40}Ar-^{39}Ar reference age for the Durango apatite (U-Th)/He and fission-track dating standard. Chemical Geology 214, 249–263. https://doi.org/10.1016/j.chemgeo.2004.10.002.

Metelkin, D.V., Vernikovsky, V.A., Kazansky, A.Y., 2012. Tectonic evolution of the Siberian paleocontinent from the Neoproterozoic to the Late Mesozoic: paleomagnetic record and reconstructions. Russian Geology and Geophysics 53, 675–688. https://doi.org/10.1016/j.rgg.2012.05.006.

Metelkin, D.V., Vernikovsky, V.A., Kazansky, A.Y., Wingate, M.T.D., 2010. Late Mesozoic tectonics of Central Asia based on paleomagnetic evidence. Gondwana Research 18, 400–419. https://doi.org/10.1016/j.gr.2009.12.008.

Molnar, P., Tapponier, P., 1975. Cenozoic tectonics of Asia: effects of a continental collision. Science (80-) 189.

Paton, C., Hellstrom, J., Paul, B., Woodhead, J., Hergt, J., 2011. Iolite: freeware for the visualisation and processing of mass spectrometric data. Journal of Analytical Atomic Spectrometry 26, 2508. https://doi.org/10.1039/c1ja10172b.

Reiners, P.W., Spell, T.L.S., Nicolescu, S., Zanetti, K.A., 2004. Zircon (U-Th)/He thermochronometry: He diffusion and comparisons with ^{40}Ar/^{39}Ar dating. Geochimica et Cosmochimica Acta 68, 1857–1887. https://doi.org/10.1016/j.gca.2003.10.021.

Roger, F., Jolivet, M., Malavieille, J., 2010. The tectonic evolution of the Songpan-Garzê (North Tibet) and adjacent areas from Proterozoic to Present: a synthesis. Journal of Asian Earth Sciences 39, 254–269. https://doi.org/10.1016/j.jseaes.2010.03.008.

Rolland, Y., Alexeiev, D.V., Kröner, A., Corsini, M., Loury, C., Monié, P., 2013. Late Palaeozoic to Mesozoic kinematic history of the Talas-Ferghana strike-slip fault (Kyrgyz West Tianshan) as revealed by ^{40}Ar/^{39}Ar dating of syn-kinematic white mica. Journal of Asian Earth Sciences 67–68, 76–92. https://doi.org/10.1016/j.jseaes.2013.02.012.

Schoene, B., Bowring, S.A., 2006. U-Pb systematics of the McClure Mountain syenite: thermochronological constraints on the age of the ^{40}Ar/^{39}Ar standard MMhb. Contributions to Mineralogy and Petrology 151, 615–630. https://doi.org/10.1007/s00410-006-0077-4.

Schwab, M., Ratschbacher, L., Siebel, W., Mcwilliams, M., Minaev, V., Lutkov, V., Chen, F., Stanek, K., Nelson, B., Frisch, W., Wooden, J.L., 2004. Assembly of the Pamirs: age and origin of magmatic belts from the southern Tien Shan to the southern Pamirs and their relation to Tibet. Tectonics 23. https://doi.org/10.1029/2003TC001583.

Seltmann, R., Konopelko, D., Biske, G., Divaev, F., Sergeev, S., 2011. Hercynian post-collisional magmatism in the context of Paleozoic magmatic evolution of the Tien Shan orogenic belt. Journal of Asian Earth Sciences 42, 821–838. https://doi.org/10.1016/j.jseaes.2010.08.016.

Sengör, A.M.C., 1984. The Cimmeride orogenic system and the tectonics of Eurasia. Geological Society of America Bulletin 195, 77.

Sengör, A.M.C., Natalin, B.A., Burtman, V.S., 1993. Evolution of the Altaid Tectonic collage and Palaeozoic crustal growth in Eurasia. Nature 364. https://doi.org/10.1038/364299a0.

Sobel, E.R., 1999. Basin analysis of the Jurassic – Lower Cretaceous southwest Tarim basin, northwest China. Geological Society of America Bulletin 111, 709–724.

Sobel, E.R., Chen, J., Heermance, R.V., 2006a. Late Oligocene–Early Miocene initiation of shortening in the Southwestern Chinese Tian Shan: implications for Neogene shortening rate variations. Earth and Planetary Science Letters 247, 70–81. https://doi.org/10.1016/j.epsl.2006.03.048.

Sobel, E.R., Dumitru, T.A., 1997. Thrusting and exhumation around the margins of the western Tarim basin during the India-Asia collision. Journal of Geophysical Research – Solid Earth 102, 5043–5063. https://doi.org/10.1029/96JB03267.

Sobel, E.R., Oskin, M., Burbank, D., Mikolaichuk, A., 2006b. Exhumation of basement-cored uplifts: example of the Kyrgyz Range quantified with apatite fission track thermochronology. Tectonics 25. https://doi.org/10.1029/2005TC001809.

Tang, W., Zhang, Z., Li, J., Li, K., Luo, Z., Chen, Y., 2015. Mesozoic and Cenozoic uplift and exhumation of the Bogda Mountain, NW China: evidence from apatite fission track analysis. Geoscience Frontiers 6, 617–625. https://doi.org/10.1016/j.gsf.2014.04.006.

Thomas, J.C., Perroud, H., Cobbold, P.R., Burtman, V.S., Chauvin, A., Perroud, H., Cobbold, P.R., Bazhenov, M.L., Burtman, V.S., Sadybakasov, E., Chauvin, A., 1993. A paleomagnetic study of tertiary formations from the Kyrgyz Tien-Shan and its tectonic implications. Journal of Geophysical Research 98, 9571–9589. https://doi.org/10.1029/92JB02912.

Trifonov, V.G., Korzhenkov, A.M., Omar, K.M., 2015. Recent geodynamics of major strike-slip zones. Geodesy and Geodynamics 6, 361–383. https://doi.org/10.1016/j.geog.2015.06.003.

Van der Voo, R., Levashova, N.M., Skrinnik, L.I., Kara, T.V., Bazhenov, M.L., 2006. Late orogenic, large-scale rotations in the Tien Shan and adjacent mobile belts in Kyrgyzstan and Kazakhstan. Tectonophysics 426, 335–360. https://doi.org/10.1016/j.tecto.2006.08.008.

Vassallo, R., Jolivet, M., Ritz, J.F., Braucher, R., Larroque, C., Sue, C., Todbileg, M., Javkhlanbold, D., 2007. Uplift age and rates of the Gurvan Bogd system (Gobi-Altay) by apatite fission track analysis. Earth and Planetary Science Letters 259, 333–346. https://doi.org/10.1016/j.epsl.2007.04.047.

Vermeesch, P., 2009. RadialPlotter: a Java application for fission track, luminescence and other radial plots. Radiation Measurements 44, 409–410. https://doi.org/10.1016/j.radmeas.2009.05.003.

Please cite this article in press as: Nachtergaele, S., et al., Meso-Cenozoic tectonic evolution of the Talas-Fergana region of the Kyrgyz Tien Shan revealed by low-temperature basement and detrital thermochronology, Geoscience Frontiers (2017), https://doi.org/10.1016/j.gsf.2017.11.007

Wack, M.R., Gilder, S.A., Macaulay, E.A., Sobel, E.R., Charreau, J., Mikolaichuk, A., 2014. Cenozoic magnetostratigraphy and magnetic properties of the southern Issyk-Kul basin, Kyrgyzstan. Tectonophysics 629, 14–26. https://doi.org/10.1016/j.tecto.2014.03.030.

Wagner, G.A., Van den haute, P., 1992. Fission-track Dating. Springer.

Wang, Q., Li, S., Du, Z., 2009. Differential uplift of the Chinese Tianshan since the Cretaceous: constraints from sedimentary petrography and apatite fission-track dating. International Journal of Earth Sciences 98, 1341–1363. https://doi.org/10.1007/s00531-009-0436-2.

Wang, Y., Cai, K., Sun, M., Xiao, W., De Grave, J., Wan, B., Bao, Z., 2017. Tracking the multi-stage exhumation history of the western Chinese Tianshan by Apatite Fission Track (AFT) dating: implication for the preservation of epithermal deposits in the ancient orogenic belt. Ore Geology Reviews. https://doi.org/10.1016/j.oregeorev.2017.04.011.

Watson, M.P., Hayward, A.B., Parkinson, D.N., Zhang, Z.M., 1987. Plate tectonic history, basin development a+nd petroleum source rock deposition onshore China. Marine and Petroleum Geology 4, 205–225. https://doi.org/10.1016/0264-8172(87)90045-6.

Wilhem, C., Windley, B.F., Stamp, G.M., 2012. The Altaids of Central Asia: a tectonic and evolutionary innovative review. Earth-Science Reviews 113, 303–341. https://doi.org/10.1016/j.earscirev.2012.04.001.

Windley, B.F., Alexeiev, D.V., Xiao, W., Kröner, A., Badarch, G., 2007. Tectonic models for accretion of the Central Asian Orogenic Belt. Journal of the Geological Society, London 164, 31–47.

Xiao, W., Han, C., Yuan, C., Sun, M., Lin, S., Chen, H., Li, Z., Li, J., Sun, S., 2008. Middle Cambrian to Permian subduction-related accretionary orogenesis of Northern Xinjiang, NW China: implications for the tectonic evolution of central Asia. Journal of Asian Earth Sciences 32, 102–117. https://doi.org/10.1016/j.jseaes.2007.10.008.

Yang, W., Dupont-Nivet, G., Jolivet, M., Guo, Z., Bougeois, L., Bosboom, R., Zhang, Z., Zhu, B., Heilbronn, G., 2015. Magnetostratigraphic record of the early evolution of the southwestern Tian Shan foreland basin (Ulugqat area), interactions with Pamir indentation and India–Asia collision. Tectonophysics 644–645, 122–137. https://doi.org/10.1016/j.tecto.2015.01.003.

Yang, W., Jolivet, M., Dupont-Nivet, G., Guo, Z., 2014. Mesozoic – Cenozoic tectonic evolution of southwestern Tian Shan: evidence from detrital zircon U/Pb and apatite fission track ages of the Ulugqat area, Northwest China. Gondwana Research 26, 986–1008. https://doi.org/10.1016/j.gr.2013.07.020.

Yang, Y.T., Guo, Z.X., Song, C.C., Li, X.B., He, S., 2015. A short-lived but significant Mongol-Okhotsk collisional orogeny in latest Jurassic-earliest Cretaceous. Gondwana Research 28, 1096–1116. https://doi.org/10.1016/j.gr.2014.09.010.

Yin, A., Harrison, T.M., 2000. Geologic evolution of the Himalayan-Tibetan Orogen. Annual Review of Earth and Planetary Sciences 28, 211–280.

Yin, W., Fan, Z., Zheng, J., Yin, J., Zhang, M., Sheng, X., Guo, J., Li, Q., Lin, Y., 2012. Characteristics of strike-slip inversion structures of the Karatau fault and their petroleum geological significances in the South Turgay Basin, Kazakhstan. Petroleum Science 9, 444–454. https://doi.org/10.1007/s12182-012-0228-3.

Zhang, Z., Zhu, W., Zheng, D., Zheng, B., Yang, W., 2016. Apatite fission track thermochronology in the Kuluketage and Aksu areas, NW China: implication for tectonic evolution of the northern Tarim. Geoscience Frontiers 7, 171–180. https://doi.org/10.1016/j.gsf.2015.08.007.

Zhu, D., Zhao, Z., Niu, Y., Mo, X., Chung, S., Hou, Z., 2011. The Lhasa Terrane: record of a microcontinent and its histories of drift and growth. Earth and Planetary Science Letters 301, 241–255. https://doi.org/10.1016/j.epsl.2010.11.005.

Zhu, D.C., Li, S.M., Cawood, P.A., Wang, Q., Zhao, Z.D., Liu, S.A., Wang, L.Q., 2016. Assembly of the Lhasa and Qiangtang terranes in central Tibet by divergent double subduction. Lithos 245, 7–17. https://doi.org/10.1016/j.lithos.2015.06.023.

Zorin, Y.A., 1999. Geodynamics of the western part of the Mongolia-Okhotsk collisional belt, Trans-Baikal region (Russia) and Mongolia. Tectonophysics 306, 33–56. https://doi.org/10.1016/S0040-1951(99)00042-6.

Please cite this article in press as: Nachtergaele, S., et al., Meso-Cenozoic tectonic evolution of the Talas-Fergana region of the Kyrgyz Tien Shan revealed by low-temperature basement and detrital thermochronology, Geoscience Frontiers (2017), https://doi.org/10.1016/j.gsf.2017.11.007